Growth-independent cross-feeding modifies boundaries for coexistence in a bacterial mutualism

Running title: Growth-independent metabolism in a mutualism

Alexandra L. McCully*, Breah LaSarre*, and James B. McKinlay[#]

*Both authors contributed equally to this work

[#]Corresponding author. 1001 E 3rd Street, Jordan Hall, Bloomington, IN 47405

Phone: 812-855-0359

Fax: 812- 855-6705

Email: jmckinla@indiana.edu

Significance statement.

Microbial mutualisms, such as those enforced by cross-feeding of metabolites, are widespread yet invariably face periods of nutrient limitation. Here we use experimental and theoretical approaches involving a synthetic community of two bacterial species to identify growth-independent maintenance metabolism as an important mechanism by which mutualistic cross-feeding can establish and persist in the face of nutrient limitation.

Summary

Nutrient cross-feeding can stabilize microbial mutualisms, including those important for carbon cycling in nutrient-limited anaerobic environments. It remains poorly understood how nutrient limitation within natural environments impacts mutualist growth, cross-feeding levels, and ultimately mutualism dynamics. We examined the effects of nutrient limitation within a mutualism using theoretical and experimental approaches with a synthetic anaerobic coculture pairing fermentative *Escherichia coli* and phototrophic *Rhodopseudomonas palustris*. In this coculture, *E. coli* and *R. palustris* resemble an anaerobic food web by cross-feeding essential carbon (organic acids) and nitrogen (ammonium), respectively. Organic acid cross-feeding stemming from *E. coli* fermentation can continue in a growth-independent manner during nutrient limitation, while ammonium cross-feeding by *R. palustris* is growth-dependent. When ammonium cross-feeding was limited, coculture trends changed yet coexistence persisted under both homogenous and heterogenous conditions. Theoretical modeling indicated that growth-independent fermentation was crucial to sustain cooperative growth under conditions of low nutrient exchange. In contrast to stabilization at low cell density, growth-independent fermentation inhibited mutualistic growth when the *E. coli* cell density was adequately high relative to that of *R. palustris*. Thus, growth-independent fermentation can conditionally stabilize or destabilize a mutualism, indicating the potential importance of growth-independent metabolism for nutrient-limited mutualistic communities.

Introduction

Mutualistic cross-feeding interactions between microbes crucially impact diverse processes ranging from human health (Flint *et al.*, 2007; Ramsey and Whiteley, 2009; Hammer *et al.*, 2014) to biogeochemical cycles (McInerney *et al.*, 2010; Morris *et al.*, 2013; Durham *et al.*, 2015). Within most environments, microbial communities experience prolonged periods of nutrient limitation (Lever *et al.*, 2015). In general, bacteria tolerate nutrient limitation by modulating their growth and metabolism (Lee *et al.*, 1976; Wanner and Egli, 1990; Russell and Cook, 1995; Ferenci, 2001; Rittershaus *et al.*, 2013). Sub-optimally growing and even non-growing cells continue to generate maintenance energy, that is energy required for any process that is not directly used for synthesizing and polymerizing biosynthetic precursors, and thereby survive by retaining partial metabolic activity (Wanner and Egli, 1990; Russell and Cook, 1995; Hoehler and Jørgensen, 2013; Rittershaus *et al.*, 2013). We hereon refer to this growth-independent metabolic activity for cell maintenance as maintenance metabolism. While maintenance metabolism occurs during growth, it can make up the majority of metabolic activity in slow-growing and especially non-growing cells. As a consequence of maintenance metabolism being independent of growth, the overall metabolic activity of a cell does not decline proportionately to growth rate during nutrient limitation.

For fermentative microbes, the transformation of energy into ATP and a proton motive force is intimately associated with the excretion of fermentation products. During nutrient limitation, the maintenance metabolism of fermentative microbes is associated with product excretion, albeit at a lower rate than during growth. For example, in the absence of electron acceptors, and starved for essential elements (i.e., nitrogen or sulfur), *Escherichia coli* generates energy by fermenting glucose in a growth-independent manner (Wanner and Egli, 1990; LaSarre

et al., 2017). Fermentative microbes serve pivotal roles within natural anaerobic food webs, wherein their excreted products serve as nutrients for other microbes. It is possible that fermentation products associated with maintenance metabolism could serve to cross-feed other microbes and thereby influence the initiation and/or endurance of microbial mutualisms under growth-limiting conditions. Nonetheless, most microbial cross-feeding studies view nutrient release as being tightly coupled to growth. While mutualism flux balance models tend to include growth-independent maintenance parameters (Harcombe *et al.*, 2014; Chubiz *et al.*, 2015), most other mutualism models do not, and few studies have examined the impact of growth-independent cross-feeding on mutualism dynamics (Megee III *et al.*, 1972; Shou *et al.*, 2007; Stolyar *et al.*, 2007). Studying mutualistic cross-feeding in natural environments can be challenging due to environmental and genetic stochasticity. Synthetic microbial communities, or cocultures, offer an alternative approach that mimics key aspects of natural communities while providing a greater degree of experimental control (Momeni *et al.*, 2011; Ponomarova and Patil, 2015; Lindemann *et al.*, 2016; Widder *et al.*, 2016). We previously developed a bacterial coculture to facilitate the study of mutualistic cross-feeding in anaerobic environments (LaSarre *et al.*, 2017) (Fig. 1). Our coculture resembles other fermenter-photoheterotroph cocultures, which have primarily been studied for converting plant-derived sugars into H_2 biofuel (Odom and Wall, 1983; Fang *et al.*, 2006; Ding *et al.*, 2009; Sun *et al.*, 2010). However, unlike previous systems, our coculture enforces stable coexistence through bi-directional cross-feeding of essential nutrients. Specifically, *E. coli* ferments sugars to excreted organic acids, providing essential carbon and electrons for a genetically engineered *Rhodopseudomonas palustris* strain (Nx). *R. palustris* Nx has a NifA* mutation (McKinlay and Harwood, 2010) that results in NH_4^+ excretion during N_2 fixation, providing essential nitrogen for *E. coli* (LaSarre *et al.*, 2017). We

previously used our coculture to examine the effects of increased NH_4^+ cross-feeding on coculture dynamics (LaSarre *et al.*, 2017). In that study, theoretical modeling suggested that coexistence would persist even at very low NH_4^+ excretion levels (LaSarre *et al.*, 2017). This prediction prompted us to ask herein, how does this mutualism contend with limitation of cross-fed nutrients?

Using theoretical and experimental approaches, we show that fermentative maintenance metabolism is crucial for maintaining cooperative growth during limitation of cross-fed NH_4^+. Conversely, fermentative maintenance metabolism is detrimental to the mutualism under circumstances where the *E. coli* cell density far exceeds that of *R. palustris*, as the otherwise low maintenance metabolism rate is magnified and leads to an inhibitory acidification of the environment. Thus, growth-independent cross-feeding conditionally influences this mutualism in positive and negative manners and thereby sets both the lower and upper thresholds for cooperation.

Results

Coexistence is maintained at reduced NH_4^+ cross-feeding levels. Previously, we found that stable coexistence and reproducible trends in our mutualistic coculture were dependent on the transfer of NH_4^+ from *R. palustris* Nx to *E. coli* (LaSarre *et al.*, 2017). Adding NH_4^+ to the medium broke the dependency of *E. coli* on *R. palustris* and resulted in *E. coli* domination due to its higher intrinsic growth rate relative to that of *R. palustris*. Thus, the NH_4^+ cross-feeding level controls the *E. coli* growth rate within the mutualism. We were intrigued that theoretical modeling predicted that mutualism coexistence would be maintained even at very low NH_4^+

cross-feeding levels, as such levels should severely limit or event halt *E. coli* growth (Supporting Information Fig. S1A) (LaSarre *et al.*, 2017).

To test this prediction, we sought to experimentally manipulate *R. palustris* NH_4^+ excretion. In our previous study, cocultures were grown under a 100% N_2 headspace with shaking to promote gas exchange and homogenous conditions (LaSarre *et al.*, 2017). Under these conditions, the NifA* mutation presumably results in a rate of N_2 fixation that exceeds the rate of biosynthesis, leading to excretion of excess NH_4^+. We therefore reasoned that limiting the N_2 supply in shaken cocultures could lower the rate of NH_4^+ production by nitrogenase, and consequently *R. palustris* Nx would retain a larger portion of the NH_4^+ for biosynthesis and excrete less. To limit the N_2 concentration, we injected N_2 into sealed coculture tubes with an argon-filled headspace to reach a final concentration of 18% N_2, a concentration we estimated would be close to limiting *R. palustris* growth in our coculture conditions, based on the elemental composition of *R. palustris* (McKinlay and Harwood, 2010). In agreement with our expectation, supernatants from shaking *R. palustris* monocultures with 18% N_2 contained half as much NH_4^+ compared to 100% N_2 monocultures (Fig. 2). We concluded that N_2 limitation was a suitable approach to manipulate NH_4^+ excretion levels.

To examine the degree of N_2 limitation that would support coexistence, we grew cocultures with a range of N_2 concentrations and monitored H_2 yields and growth rates. We used H_2 yield as a proxy for N_2 limitation because nitrogenase produces more H_2 and less NH_4^+ as N_2 becomes limiting (Hoffman *et al*., 2013). When nitrogenase is saturated with N_2, one mole of H_2 is obligately produced for every mole of N_2 converted into 2 NH_4^+ (Eq 1). In the absence of N_2, nitrogenase continues to oxidize electron carriers and acts as an ATP-powered hydrogenase,

producing H_2 as the sole product (Eq 2). Under sub-saturating N_2 conditions, the stoichiometric amounts of NH_4^+ and H_2 produced would be somewhere between Eqs. 1 and 2.

Eq 1. $N_2 + 10H^+ + 8e^- + 16\ ATP \rightarrow 2NH_4^+ + H_2 + 16\ ADP$

Eq 2. $8H^+ + 8e^- + 16\ ATP \rightarrow 4H_2 + 16\ ADP$

Thus, progressively decreased N_2 availability should result in less NH_4^+ excretion and more H_2 production. Unlike NH_4^+, H_2 accumulates in coculture, making it a convenient compound to assess whether *R. palustris* cells in coculture are experiencing sub-saturating N_2 conditions. N_2-limited cocultures were incubated horizontally with shaking to promote a homogeneous environment. As expected, the coculture H_2 yield increased as N_2 concentration decreased, but the yield plateaued at N_2 concentrations below 15% (Fig. 3A). Below 15% N_2, *R. palustris* might redirect electrons away from H_2 production towards other products like polyhydroxybutyrate, as has been observed as part of a nitrogen-starvation response in *R. palustris* (McKinlay *et al.*, 2014). N_2 limitation was also evident from the coculture growth rate, which decreased as the N_2 concentration decreased (Fig. 3B; Supporting Information Fig. S2A). Notably, cocultures still grew at the lowest concentration of N_2 tested (6% headspace N_2; Fig. 3B), indicating that sufficient NH_4^+ was cross-fed to permit mutualistic growth.

Moving forward, we focused on 18% N_2 to characterize how lower NH_4^+ cross-feeding affected coculture dynamics. We chose 18% N_2 as a concentration where nitrogen-limitation impacted coculture trends but without causing the observed H_2 yield plateau (Fig. 3). Previous model simulations predicted that decreasing NH_4^+ cross-feeding would result in a decrease in the *E. coli* population within the coculture (Supporting Information Fig. S1A). In agreement with this, we observed that *E. coli* made up 5% of the population in the cocultures with 18% N_2, which was significantly lower than the 9% *E. coli* frequency observed in cocultures with 100%

N_2 (Fig. 4A) (LaSarre *et al.*, 2017). To assess coculture reproducibility, we performed serial transfers of cocultures with 18% N_2. Growth yield, H_2 yield, and growth rates were all reproducible across serial transfers (Fig. 4), indicating that coexistence was stable despite the lower level of NH_4^+ cross-feeding.

Coexistence is maintained in heterogeneous environments that decrease NH_4^+ cross-feeding. Spatial structuring can impact microbial mutualistic interactions, and is even required for coexistence in some cases (Kim *et al.*, 2008; Harcombe, 2010; Summers *et al.*, 2010; Hom and Murray, 2014). In other cases, well-mixed environments sufficiently promote cooperative relationships (Hillesland and Stahl, 2010; Mee *et al.*, 2014; Pande *et al.*, 2014). We hypothesized that the homogeneous environment in our shaking cocultures might dampen the impact of low NH_4^+ cross-feeding levels. Thus, we examined whether a heterogeneous environment would affect coexistence within N_2-limited cocultures.

One way to induce a heterogeneous environment is by incubating in static conditions, wherein cocultures are not agitated. Static incubation results in settling of cells to the bottom of the culture tube in both cocultures and *R. palustris* monocultures, which we expected would result in a gradient of N_2 availability (Supporting Information Fig. S3). As N_2 diffuses into the medium, *R. palustris* cells closer to surface would be first to encounter and utilize the N_2, which would diminish the N_2 available to *R. palustris* cells towards the bottom of the tube. The N_2-limited cells at the bottom of the tube would therefore produce less NH_4^+ and more H_2, leading to less NH_4^+ excretion by the *R. palustris* population overall (Supporting Information Fig. S3). Confirming this hypothesis, static *R. palustris* Nx monocultures with 100% N_2 grew to a similar density as when shaken, but showed less NH_4^+ excretion, similar to what was observed in

monocultures shaken with 18% N_2 (Fig. 2). This trend was exacerbated in static *R. palustris* Nx monocultures with only 18% N_2, which also showed lower cell densities (Fig. 2), likely due to a greater redirection of electrons to H_2 rather than to biosynthesis, the major *R. palustris* electron sink when nitrogen is abundant (McKinlay *et al*., 2014).

To determine how heterogeneous environments affected coculture trends under N_2 limitation, we performed serial transfers of cocultures grown under static conditions with either 100% or 18% N_2 in the headspace, every 2 or 4 weeks, respectively. These longer incubation times were necessary to achieve similar final cell densities between shaking and static environments. Static cocultures with 100% N_2 had higher H_2 yields than shaken cocultures with 100% N_2 (Fig. 5A). This was expected given that an *R. palustris* subpopulation was experiencing N_2 limitation (Eq 1 vs 2). Supplying only 18% N_2 in static cocultures amplified this trend further (Fig. 5A). In agreement with prior simulations (Supporting Information Fig. S1A), *R. palustris* growth yields remained similar or increased in response to N_2 limitation whereas *E. coli* growth yields decreased (Fig. 5B). Coexistence was maintained over serial transfers regardless of N_2 availability (Fig. 5B). Collectively, these data demonstrate the robustness of our coculture to low NH_4^+ cross-feeding levels in both homogenous and heterogeneous environments.

Fermentation products from maintenance metabolism are crucial for coexistence at low cross-feeding levels. In coculture, *R. palustris* growth yields depend on carbon acquisition from *E. coli*. The relative consistency of *R. palustris* final cell densities despite lower *E. coli* cell densities during N_2 limitation (Fig. 5) led us to hypothesize that fermentation associated with *E. coli* maintenance metabolism could be sustaining *R. palustris* during N_2 limitation. By this hypothesis, NH_4^+-limited *E. coli* would grow at a slower rate but would continue to use

fermentation for maintenance energy; consequently, *R. palustris* would receive a slower but continuous supply of organic acids for growth and N_2 fixation. Ultimately, *E. coli* would assimilate less glucose, as a larger proportion would be used for maintenance, whereas *R. palustris* would receive a similar or even greater amount of carbon from *E. coli*. This hypothesis in turn implies that fermentative maintenance metabolism by *E. coli* is important for sustaining *R. palustris* metabolism and thereby coculture viability during N_2 limitation.

To empirically test whether fermentative maintenance metabolism can support *R. palustris* growth, we first examined the most extreme condition by completely preventing *E. coli* growth. To prevent *E. coli* growth we made an *E. coli* histidine auxotroph (ΔHisB). Our coculture medium does not contain amino acids, so *E. coli* ΔHisB cannot grow regardless of NH_4^+ cross-feeding. In cocultures with *E. coli* ΔHisB, glucose was slowly consumed, the *E. coli* ΔHisB cell density declined, and the *R. palustris* cell density increased (Fig. 6A). These results suggested that fermentative maintenance metabolism supported *R. palustris* growth. However, metabolism of cellular material released by lysed cells can be important for maintaining microbial populations through periods of starvation (Finkel, 2006; Rozen *et al.*, 2009). Therefore, we also considered cell lysis of *E. coli* ΔHisB as a carbon source for *R. palustris.* We estimated how much carbon could be released from *E. coli* cell lysis based on the observed decline in CFUs and elemental compositions of each bacterium (see Methods). Our estimates suggest that all of the carbon from dead *E. coli* cells could only account for ~0.4% of the carbon required for the amount of *R. palustris* growth observed (Fig. 6B). In contrast, there was more than enough carbon from the glucose consumed in coculture to account for all the *R. palustris* biomass observed (Fig. 6B). We therefore concluded that fermentative maintenance metabolism can contribute to the cross-feeding of carbon within the mutualism.

Based on the above result we reasoned that fermentative maintenance metabolism was also likely contributing to coexistence in N_2-limited cocultures with wild-type *E. coli*. However, gauging the impact of fermentative maintenance metabolism during partial starvation conditions is experimentally infeasible as the essential nature of maintenance metabolism means it cannot be genetically eliminated. We therefore turned to modeling to assess the importance of fermentative maintenance metabolism during N_2 limitation that permits slow *E. coli* growth. We first modified our previous model (LaSarre *et al.*, 2017) to account for the effects of N_2 limitation on the shift from NH_4^+ to H_2 production by *R. palustris* (SyFFoN_v2; Supporting Information Methods, Fig. S4-6, and Table S2). The model does not take into account ATP availability for the nitrogenase reactions (Eq.1 and 2); we assumed that ATP is readily available during N_2 limitation since *R. palustris* produces high concentrations of H_2 when completely starved for nitrogen but provided with light (McKinlay *et al*., 2014). We then adjusted SyFFoN_v2 parameters to simulate growth rate and metabolite yield data observed at various N_2 concentrations (Fig. 3 and Supporting Information Fig. S2 and S4-6). In doing so we found that parameters based on *E. coli* monoculture data (LaSarre *et al.*, 2017) could not accurately simulate coculture growth rates observed at low N_2 concentrations. Rather, *E. coli* maintenance metabolism had to be increased by up to two-orders of magnitude to more accurately simulate empirical growth rates (Fig. 3B and Supporting Information Table S2). The need for these changes to more accurately simulate observed trends suggests that *R. palustris* consumption of fermentation products pulls *E. coli* fermentation by minimizing end-product inhibition, analogous to what has been observed in other fermentative cross-feeding systems (Iannotti *et al.*, 1973; Hillesland and Stahl, 2010). SyFFoN_v2 accurately predicted H_2 yields (Fig. 3A), normalized growth rates (Fig. 3B), and product yields (Supporting Information Fig. S2) between

15% and 100 % N_2. At N_2 levels below 15%, *R. palustris* likely undergoes a starvation response resulting in physiological effects that our model does not predict. We also verified that SyFFoN_v2 could reproduce trends from our previous study (LaSarre *et al.*, 2017), namely the effects of added NH_4^+ (Supporting Information Fig. S7) and varying the *R. palustris* NH_4^+ excretion levels (Supporting Information Fig. S1A).

To examine how fermentative maintenance metabolism influenced this mutualism, we used SyFFoN_v2 to simulate the effect of N_2 limitation on population dynamics in the presence or absence of *E. coli* maintenance metabolism (Fig. 7). With *E. coli* maintenance metabolism included, the model predicted that mutualistic growth would be sustained even as N_2 concentrations approached zero. *E. coli* final cell densities were predicted to decline as N_2 levels fall below ~30% while *R. palustris* final cell densities would decline as N_2 levels fall below ~20% (Fig. 7A). In the absence of *E. coli* maintenance metabolism, simulations predicted a truncated range of N_2 concentrations that would support coculture growth (Fig. 7B). In fact, the simulations suggested that *E. coli* maintenance metabolism is necessary at N_2 concentrations where we observed reproducible coculture growth trends (Fig. 7). The model predicted similar trends when NH_4^+ excretion levels were varied in place of N_2 availability (Supporting Information Fig. S1).

A closer inspection of simulated cross-feeding levels revealed why coculture growth at low N_2 concentrations (or low NH_4^+ cross-feeding levels) required fermentative maintenance metabolism. At high N_2 levels (100% N_2), growth-coupled fermentation alone is sufficient to support coculture growth, as any increase in populations results in progressively more metabolites exchanged over time (Supporting Information Fig. S8A). However, near the transitional N_2 concentration where coculture growth is predicted to fail in the absence of

fermentative maintenance metabolism (28% N_2), metabolite excretion levels decrease as populations grow, resulting in continuously less essential resources for subsequent generations despite available glucose; in other words, cross-feeding spirals into a cycle of diminishing returns (Supporting Information Fig. S8B). Our data indicate that fermentative maintenance metabolism can circumvent diminishing returns. Fermentation products will always be produced, and thus *R. palustris* will eventually grow to a density that collectively excretes sufficient NH_4^+ to allow for *E. coli* growth. Indeed, when *E. coli* maintenance metabolism is included at 28% N_2, growth-independent cross-feeding by *E. coli* stimulates sufficient reciprocal NH_4^+ excretion to sustain coculture growth (Supporting Information Fig. S8C). These simulations strongly suggest that fermentative maintenance metabolism permits cooperative growth at low NH_4^+ excretion levels that would otherwise be insufficient.

***E. coli* maintenance metabolism prevents cooperative growth at high *E. coli* cell densities.** On a per cell basis, fermentation product excretion due to maintenance metabolism is considerably slower than that associated with growth (Russell and Cook, 1995). However, we reasoned that a high *E. coli* cell density could amplify this low rate such that organic acid production would be substantial at a population level. We previously demonstrated that dose-dependent toxicity governs mutualism dynamics in our coculture; specifically, organic acids play a beneficial role as a carbon source for *R. palustris*, but a detrimental role when they accumulate enough to acidify the medium (LaSarre *et al.*, 2017). Thus, we hypothesized that if *E. coli* cell densities were sufficiently high, the collective fermentation rate attributed to maintenance metabolism alone might destabilize the mutualism by producing organic acids faster than the smaller *R. palustris* population could consume them, resulting in growth-inhibiting acidification.

To test this hypothesis, we first simulated coculture growth from different initial species densities using SyFFoN_v2. The model correctly predicted that a common equilibrium would be reached from a wide range of initial *E. coli* densities (Fig. 8A) (LaSarre *et al.*, 2017). However, in agreement with our hypothesis, the model also predicted a maximum initial *E. coli* density that would allow cooperative growth (Fig. 8A). An upper limit was experimentally verified, albeit at a lower *E. coli* density than what was predicted (Fig. 8A). At an initial *E. coli* density of ~2 x 10^9 CFU / ml, the pH reached acidic levels known to prevent *R. palustris* growth and metabolism (Fig. 8A) (LaSarre *et al.*, 2017). As a result, neither species' population increased (Fig. 8A). These results contradicted predictions when maintenance metabolism was omitted from the model, as there was no predicted initial *E. coli* density that would prevent cooperative growth (Fig. 8B).

While SyFFoN_v2 qualitatively predicted that the maintenance metabolism from high initial *E. coli* cell density would lead to growth-inhibiting acidification, it was quantitatively inaccurate (Fig. 8A). This prediction used maintenance metabolism rates that were based on data from *E. coli* cells that had been adapted to non-growing conditions for 1 day. However, fermentation rates during days 1-7 were 2- to 10-fold slower than those observed over days 0-1; thus, the inaccuracy could stem from an underestimation of the early maintenance fermentation rate (Supporting Information Fig. S9). To explore this possibility, we calculated the level of organic acids that would accumulate in 24 h for a given initial *E. coli* cell density using fermentation rates determined during the first day of *E. coli* cell suspensions (Supporting Information Fig. S9). These organic acid levels were then entered as initial values into SyFFoN_v2 to account for organic acid production during the first 24 h, and batch cultures were then simulated with all the other parameter values the same as used for Fig. 8A. The simulations

indicate that when the initial *E. coli* cell density is low, a rapid early rate of organic acid production leads to negligible organic acid accumulation and thus the population trends are unaffected (Fig. 8C). However, when the initial *E .coli* cell density is high, a rapid early rate of organic acid production can lead to substantial organic acid accumulation and better approximate the upper *E. coli* cell density that would prevent coculture growth (Fig 8C). A potentially compounding factor to help explain the discrepancy between simulated and observed inhibitory initial *E. coli* levels is that once inhibitory acid levels are reached, cell death will likely occur; SyFFoN_v2 does not simulate cell death.

SyFFoN_v2 simulations also indicated that it is the initial *E. coli* cell density rather than the initial species ratio that determines if coculture growth will be prevented through dose-dependent toxicity; the inhibitory effect of high initial *E. coli* cell densities could be offset by a high initial *R. palustris* cell density enabling organic acid consumption at a rate sufficient to hamper accumulation (Fig. 8D). However, simulations suggest that an initial *R. palustris* concentration of 10^{10} cells / ml would be required to fully offset the acidification from an initial *E. coli* cell density of 10^9 cells / ml, mainly because NH_4^+cross-feeding by *R. palustris* would stimulate *E. coli* growth and thereby accelerate fermentation and organic acid accumulation. Thus, while *E. coli* maintenance metabolism is a stabilizing factor at low NH_4^+ exchange levels, it can also serve to destabilize the mutualism at high *E. coli* densities.

Discussion

In this study, we demonstrated that cross-feeding stemming from maintenance metabolism can circumstantially impede or promote mutualism. We found that mutualism destabilization by maintenance metabolism depends on dose-dependent toxicity of a cross-fed

nutrient. Specifically, destabilization occurs when a maintenance metabolism leads to the accumulation of cross-fed nutrients to levels that inhibit growth of the partner species. Destabilization of a natural mutualism linked to maintenance metabolism would require specific conditions. In our system, organic acid toxicity is relatively low, in part due to the buffered medium. Thus, an extremely high initial *E. coli* cell density was required before fermentative maintenance metabolism could inhibit cooperative growth via culture acidification. However, inhibitory effects stemming from maintenance metabolism could occur at cell densities relevant to natural systems in a less well-buffered system or if the toxicity of the cross-fed metabolite was intrinsically high. For example, notoriously toxic compounds like cyanide (Harris and Knowles, 1983) and antibiotics (Dantas *et al.*, 2008; Barnhill *et al.*, 2010) can serve as nutrients for some bacteria as long as concentrations remain low.

While the likelihood of mutualism destabilization linked to maintenance metabolism is difficult to gauge, promotion of cross-feeding relationships by maintenance metabolism is likely widespread. Vast areas of the Earth's biosphere are limited for key nutrients (Lever *et al.*, 2015), and it is well appreciated that nutrient limitation can promote cross-feeding in natural environments (Hom and Murray, 2014; Seth and Taga, 2014). However, it is poorly understood how established mutualisms respond to perturbations that limit cross-feeding itself. It is thought that exchange rates within obligate mutualisms must be sufficient to support sustained growth of both species in order to avoid eventual extinction (Shou *et al.*, 2007). Our results demonstrate that cross-feeding associated with maintenance metabolism can ease this requirement. In our system, fermentation product excretion from *E. coli* maintenance metabolism can preserve the mutualism amid unfavorable NH_4^+ exchange levels by continually cross-feeding organic acids. This persistent cross-feeding stimulates *R. palustris* growth and NH_4^+ excretion, thereby lifting

both species out of starvation. In other words, maintenance metabolism allows cross-feeding to persist and facilitates cooperative success over an extended range of excretion levels compared to metabolites whose excretion depends on growth. Given that the majority of microbes in natural environments are in a state of dormancy or low metabolic activity (Hoehler and Jørgensen, 2013; Lever *et al.*, 2015; Jørgensen and Marshall, 2016), we postulate that metabolite release is more likely to be growth-independent. As such, maintenance metabolism could better serve to initiate and maintain mutualisms in natural environments. Separately, although fermentative maintenance metabolism promoted partner growth under our study conditions, it is imaginable that mutualistic cross-feeding could purely support maintenance energy requirements in some cases, thereby promoting survival until nutrient availability improves.

Organic acids, and other fermentation products, are important metabolic intermediates in anaerobic food webs (McInerney *et al.*, 2008; Jørgensen and Marshall, 2016). Fermentative maintenance metabolism could therefore play an important role under nutrient-limiting conditions by sustaining mutualistic relationships with acetogens, methanogens, photoheterotrophs, and anaerobically respiring microbes that rely on fermentation products for carbon and electrons. However, contributions of maintenance metabolism to mutualisms need not be restricted to fermentation nor to natural environments. Generation of maintenance energy is essential. Thus, mutualistic relationships encompassing diverse lifestyles could conceivably be preserved at low metabolic rates, provided that the limiting nutrient(s) still permits the excretion of factors required to sustain partner viability. Forcing a partner into a primary state of maintenance metabolism by limiting cross-feeding could also conceivably be a selfish strategy by which a partner could capitalize on resources that are limiting to both partners without severing essential mutualistic ties. Understanding maintenance metabolism-linked cross-feeding

could also benefit industrial bioprocesses, which commonly use growth-limiting conditions to boost product yields. Indeed, growth-independent cross-feeding helped sustain our coculture during N_2-limiting conditions under which the highest H_2 yields were observed (Fig. 4 and 5). Applications of microbial consortia for industrial processes is gaining interest (Sabra *et al.*, 2010) but the effects of nutrient limitation have yet to be investigated. Clearly, the role of maintenance metabolism in fostering microbial cooperation deserves closer appraisal in both natural and applied systems.

Experimental Procedures

Strains, plasmids, and growth conditions. Strains are listed in Supporting Information Table S1. *E. coli* and *R. palustris* were cultivated on Luria-Burtani (LB) agar or defined mineral (PM) (Kim and Harwood, 1991) agar with 10 mM succinate, respectively. For determining colony forming units (CFU), LB agar or PM agar minus $(NH_4)_2SO_4$ were used for *E. coli* and *R. palustris*, respectively. Cultures were grown in 10-mL of defined M9-derived coculture medium (MDC) (LaSarre *et al.*, 2017) in 27-mL anaerobic test tubes. The medium was made anaerobic by bubbling with N_2, sealed with rubber stoppers and aluminum crimps, and then autoclaved. After autoclaving, MDC was supplemented with cation solution (1 % v/v; 100 mM $MgSO_4$ and 10 mM $CaCl_2$) and glucose (25 mM). For defined N_2 concentrations, the medium was bubbled with argon and after autoclaving defined volumes of N_2 were injected through a 0.2 micron syringe filter. All cultures were grown at 30°C either laying horizontally under a 60 W incandescent bulb with shaking at 150 rpm (shaking conditions) or upright without agitation (static conditions). Static cultures were only mixed for sampling upon inoculation and at the termination of an experiment. Thus, growth rates were not measured under static conditions.

Starter cultures were inoculated with 200 µL MDC containing a suspension of a single colonies of each species. Test cocultures were inoculated using a 1% inoculum from starter cocultures except for cocultures with the *E. coli* ΔHisB strain. For these cocultures, *E. coli* ΔHisB and *R. palustris* Nx starter monocultures were grown to equivalent cell densities, washed twice with MDC, and inoculated at a 1:1 ratio for a total of 1% inoculum. For serial transfers, cocultures were incubated for either one week (shaking), two weeks (100% N_2; static), or four weeks (18% N_2; static) before transferring a 1% stationary phase inoculum to fresh medium.

Generation of the *E. coli* ΔHisB mutant. P1 transduction was used to introduce Δ*hisB::Km* from the Keio strain JW2004-1 (Baba *et al.*, 2006) into MG1655 as described (Thomason *et al.*, 2007). The Δ*hisB::Km* mutation was confirmed by PCR and histidine auxotrophy was verified by a requirement for histidine for growth in M9 medium.

Analytical procedures. Cell density was assayed by optical density at 660 nm (OD_{660}) using a Genesys 20 visible spectrophotometer (Thermo-Fisher, Waltham, MA, USA). Growth curve readings were taken in culture tubes without sampling. Specific growth rates were determined by fitting an exponential trend line to measurements between 0.1-1.0 OD_{660} where there is linear correlation between cell density and OD_{660}. Final OD_{660} measurements (i.e., the maximum OD_{660} value corresponding to the cessation of growth) were taken in cuvettes wherein samples were diluted into the linear range as necessary. To compare cell densities between growth conditions, CFUs were converted into growth yields (CFUs per µmol glucose consumed), as N_2 limitation prevented complete glucose consumption during the assay period. H_2 and N_2 were quantified using a Shimadzu (Kyoto, Japan) gas chromatograph with a thermal conductivity detector as described (Huang *et al.*, 2010). Glucose, organic acids, and ethanol were quantified using a

Shimadzu high-performance liquid chromatograph as described (McKinlay *et al.*, 2005). NH_4^+ was quantified using an indophenol colorimetric assay as described (LaSarre *et al.*, 2017).

Calculations of carbon release due to lysis of *E. coli* ΔHisB. To estimate carbon released due to *E. coli* lysis and carbon assimilated by *R. palustris*, CFU/ml values were first used to estimate OD values using a conversion factor of 5 x 10^8 CFU/ml/OD for both species based on experimental standard curves. OD values were then converted into mg of dry cell weight (DCW)/L and then to mM carbon using published conversion factors and molecular weights from elemental compositions for *E. coli* (351 mg/L/OD, $CH_{1.77}O_{0.49}N_{0.24}$) (Neidhardt, 1987; Stockar and Liu, 1999) and *R. palustris* (625 mg/L/OD, $CH_{1.8}N_{0.18}O_{0.38}$) (McKinlay and Harwood, 2010). Dividing these values of *E. coli* carbon by *R. palustris* carbon gives the fraction of *R. palustris* growth that could be supported by *E. coli* lysis. This fraction represents an upper bound, as it is based on the liberal assumption that *R. palustris* can assimilate all carbon from a lysed *E. coli* cell.

SyFFoN_v2 model. SyFFoN_v2 was modified from a previous version of the model (LaSarre *et al.*, 2017) as described in the Supporting Information. Default parameter values and descriptions of functions are in Supporting Information Table S2 and Fig. S4-6). SyFFoN_v2 runs in R studio and is available for download at: https://github.com/McKinlab/Coculture-Mutualism.

Acknowledgements

We thank David Kysela and Amelia Randich for discussions on the model name, SyFFoN. We also thank anonymous reviewers for insightful comments, including the potential for withholding resources as a selfish strategy. This work was supported in part by the U.S. Department of Energy, Office of Science, Office of Biological and Environmental Research, under Award

Number DE-SC0008131, by the U.S. Army Research Office, grant W911NF-14-1-0411, and by the Indiana University College of Arts and Sciences. The authors declare no conflict of interest.

References

Baba, T., Ara, T., Hasegawa, M., Takai, Y., Okumura, Y., Baba, M., et al. (2006) Construction of *Escherichia coli* K-12 in-frame, single-gene knockout mutants: the Keio collection. *Mol. Syst. Biol.* **2**: 2006.0008.

Barnhill, A.E., Weeks, K.E., Xiong, N., Day, T.A., and Carlson, S.A. (2010) Identification of multiresistant *Salmonella* isolates capable of subsisting on antibiotics. *Appl. Environ. Microbiol.* **76**: 2678–2680.

Chubiz, L.M., Granger, B.R., Segrè, D., and Harcombe, W.R. (2015) Species interactions differ in their genetic robustness. *Front. Microbiol.* **6**: 1–9.

Dantas, G., Sommer, M.O.A., Oluwasegun, R.D., and Church, G.M. (2008) Bacteria Subsisting on Antibiotics. *Science.* **320**: 100–104.

Ding, J., Liu, B.F., Ren, N.Q., Xing, D.F., Guo, W.Q., Xu, J.F., and Xie, G.J. (2009) Hydrogen production from glucose by co-culture of *Clostridium butyricum* and immobilized *Rhodopseudomonas faecalis* RLD-53. *Int. J. Hydrogen Energy.* **34**: 3647–3652.

Durham, B.P., Sharma, S., Luo, H., Smith, C.B., Amin, S.A., Bender, S.J., et al. (2015) Cryptic carbon and sulfur cycling between surface ocean plankton. *Proc. Natl. Acad. Sci.* **112**: 453–457.

Fang, H., Zhu, H., and Zhang, T. (2006) Phototrophic hydrogen production from glucose by pure and co-cultures of *Clostridium butyricum* and *Rhodobacter sphaeroides*. *Int. J. Hydrogen Energy.* **31**: 2223–2230.

Ferenci, T. (2001) Hungry bacteria - definition and properties of a nutritional state. *Environ. Microbiol.* **3**: 605–611.

Finkel, S.E. (2006) Long-term survival during stationary phase: evolution and the GASP phenotype. *Nat.Rev.Microbiol.* **4**: 113–120.

Flint, H.J., Duncan, S.H., Scott, K.P., and Louis, P. (2007) Interactions and competition within the microbial community of the human colon: Links between diet and health: Minireview. *Environ. Microbiol.* **9**: 1101–1111.

Hammer, N.D., Cassat, J.E., Noto, M.J., Lojek, L.J., Chadha, A.D., Schmitz, J.E., et al. (2014) Inter- and intraspecies metabolite exchange promotes virulence of antibiotic-resistant *Staphylococcus aureus*. *Cell Host Microbe.* **16**: 531–537.

Harcombe, W. (2010) Novel cooperation experimentally evolved between species. *Evolution.* **64**: 2166–2172.

Harcombe, W.R., Riehl, W.J., Dukovski, I., Granger, B.R., Betts, A., Lang, A.H., et al. (2014) Metabolic resource allocation in individual microbes determines ecosystem interactions and spatial dynamics. *Cell Rep.* **7**: 1104–1115.

Harris, R. and Knowles, C.J. (1983) Isolation and growth of a *Pseudomonas* species that utilizes cyanide as a source of nitrogen. *J. Gen. Microbiol.* **129**: 1005–1011.

Hillesland, K.L. and Stahl, D. a (2010) Rapid evolution of stability and productivity at the origin of a microbial mutualism. *Proc. Natl. Acad. Sci. U. S. A.* **107**: 2124–9.

Hoehler, T.M. and Jørgensen, B.B. (2013) Microbial life under extreme energy limitation. *Nat. Rev. Microbiol.* **11**: 83–94.

Hoffman, B.M., Lukoyanov D., Dean, D.R., and Seefeldt, L.C. (2013) Nitrogenase: a draft mechanism. *Acc. Chem. Res.* **46**: 587–595.

Hom, E.F.Y. and Murray, A.W. (2014) Niche engineering demonstrates a latent capacity for fungal-algal mutualism *Science.* **345**: 94–98.

Huang, J.J., Heiniger, E.K., McKinlay, J.B., and Harwood, C.S. (2010) Production of hydrogen gas from light and the inorganic electron donor thiosulfate by *Rhodopseudomonas palustris*. *Appl. Environ. Microbiol.* **76**: 7717–22.

Iannotti, E.L., Kafkewit, D., Wolin, M.J., and Bryant, M.P. (1973) Glucose Fermentation Products of *Ruminococcus albus* grown in continuous culture with *Vibrio succinogenes* - Changes caused by interspecies transfer of H_2. *J. Bacteriol.* **114**: 1231–1240.

Jørgensen, B.B. and Marshall, I.P.G. (2016) Slow Microbial Life in the Seabed. *Ann. Rev. Mar. Sci.* **8**: 311–332.

Kim, H.J., Boedicker, J.Q., Choi, J.W., and Ismagilov, R.F. (2008) Defined spatial structure stabilizes a synthetic multispecies bacterial community. *Proc. Natl. Acad. Sci. U. S. A.* **105**: 18188–18193.

Kim, M.K. and Harwood, C.S. (1991) Regulation of benzoate-CoA ligase in *Rhodopseudomonas palustris*. *FEMS Microbiol. Letters.* **83**: 199–203.

LaSarre, B., McCully, A.L., Lennon, J.T., and McKinlay, J.B. (2017) Microbial mutualism dynamics governed by dose-dependent toxicity of cross-fed nutrients. *ISME J.* **11**: 337–348.

Lee, I.H., Fredrickson, A.G., and Tsuchiya, H.M. (1976) Dynamics of mixed cultures of *Lactobacillus plantarum* and *Propionibacterium shermanii*. *Biotechnol. Bioeng.* **18**: 513–26.

Lever, M.A., Rogers, K.L., Lloyd, K.G., Overmann, J., Schink, B., Thauer, R.K., et al. (2015) Life under extreme energy limitation: A synthesis of laboratory- and field-based investigations. *FEMS Microbiol. Rev.* **39**: 688–728.

Lindemann, S.R., Bernstein, H.C., Song, H.-S., Fredrickson, J.K., Fields, M.W., Shou, W., et al. (2016) Engineering microbial consortia for controllable outputs. *ISME J.* **10**: 2077–2084.

McInerney, M.J., Sieber, J.R., and Gunsalus, R.P. (2010) Syntrophy in anaerobic global carbon cycles. *Curr. Opin. Biotechnol.* **20**: 623–632.

McInerney, M.J., Struchtemeyer, C.G., Sieber, J., Mouttaki, H., Stams, A.J.M., Schink, B., et al. (2008) Physiology, ecology, phylogeny, and genomics of microorganisms capable of syntrophic metabolism. *Ann. N. Y. Acad. Sci.* **1125**: 58–72.

McKinlay, J.B. and Harwood, C.S. (2010) Carbon dioxide fixation as a central redox cofactor recycling mechanism in bacteria. *Proc. Natl. Acad. Sci. U. S. A.* **107**: 11669–75.

McKinlay, J.B., Oda, Y., Ruhl, M., Posto, A.L., Sauer, U., and Harwood, C.S. (2014) Non-growing *Rhodopseudomonas palustris* increases the hydrogen gas yield from acetate by shifting from the glyoxylate shunt to the tricarboxylic acid cycle. *J. Biol. Chem.* **4**: 1960–1970.

McKinlay, J.B., Zeikus, J.G., and Vieille, C. (2005) Insights into *Actinobacillus succinogenes* fermentative metabolism in a chemically defined growth medium. *Appl Env. Microbiol.* **71**: 6651–6656.

Mee, M.T., Collins, J.J., Church, G.M., and Wang, H.H. (2014) Syntrophic exchange in synthetic microbial communities. *Proc. Natl. Acad. Sci. U. S. A.* **111**: E2149-56.

Megee III, R.D., Drake, J.F., Fredrickson, A.G., and Tsuchiya, H.M. (1972) Studies in intermicrobial symbiosis. *Saccharomyces cerevisiae* and *Lactobacillus casei. Can. J. Microbiol.* **18**: 1722–1742.

Momeni, B., Chen, C.C., Hillesland, K.L., Waite, A., and Shou, W. (2011) Using artificial systems to explore the ecology and evolution of symbioses. *Cell. Mol. Life Sci.* **68**: 1353–

1368.

Morris, B.E.L., Henneberger, R., Huber, H., and Moissl-Eichinger, C. (2013) Microbial syntrophy: Interaction for the common good. *FEMS Microbiol. Rev.* **37**: 384–406.

Neidhardt, F.C. (1987) *Escherichia coli* and *Salmonella typhimurium* Cellular and Molecular Biology. American Society for Microbiology, Washington, DC.

Odom, J.M. and Wall, J.D. (1983) Photoproduction of H_2 from cellulose by an anaerobic bacterial coculture. *Appl Env. Microbiol.* **45**: 1300–1305.

Pande, S., Merker, H., Bohl, K., Reichelt, M., Schuster, S., de Figueiredo, L.F., et al. (2014) Fitness and stability of obligate cross-feeding interactions that emerge upon gene loss in bacteria. *ISME J.* **8**: 953–62.

Ponomarova, O. and Patil, K.R. (2015) Metabolic interactions in microbial communities: Untangling the Gordian knot. *Curr. Opin. Microbiol.* **27**: 37–44.

Ramsey, M.M. and Whiteley, M. (2009) Polymicrobial interactions stimulate resistance to host innate immunity through metabolite perception. *Proc. Natl. Acad. Sci. U. S. A.* **106**: 1578–1583.

Rittershaus, E.S.C., Baek, S.H., and Sassetti, C.M. (2013) The normalcy of dormancy: Common themes in microbial quiescence. *Cell Host Microbe.* **13**: 643–651.

Rozen, D.E., Philippe, N., Arjan De Visser, J., Lenski, R.E., and Schneider, D. (2009) Death and cannibalism in a seasonal environment facilitate bacterial coexistence. *Ecol. Lett.* **12**: 34–44.

Russell, J.B. and Cook, G.M. (1995) Energetics of bacterial growth: balance of anabolic and catabolic reactions. *Microbiol. Rev.* **59**: 48–62.

Sabra, W., Dietz, D., Tjahjasari, D., and Zeng, A.-P. (2010) Biosystems analysis and engineering

of microbial consortia for industrial biotechnology. *Eng. Life Sci.* **10**: 407–421.

Seth, E.C. and Taga, M.E. (2014) Nutrient cross-feeding in the microbial world. *Front. Microbiol.* **5**: 350.

Shou, W., Ram, S., and Vilar, J.M.G. (2007) Synthetic cooperation in engineered yeast populations. *Proc. Natl. Acad. Sci. U. S. A.* **104**: 1877–82.

Stockar, U. Von and Liu, J. (1999) Does microbial life always feed on negative entropy ? Thermodynamic analysis of microbial growth. *Biochimica et biophysica acta.* **1412**: 191–211.

Stolyar, S., Van Dien, S., Hillesland, K.L., Pinel, N., Lie, T.J., Leigh, J. a, and Stahl, D. a (2007) Metabolic modeling of a mutualistic microbial community. *Mol. Syst. Biol.* **3**: 92.

Summers, Z.M., Fogarty, H.E., Leang, C., Franks, A.E., Malvankar, N.S., and Lovley, D.R. (2010) Direct exchange of electrons within aggregates of an evolved syntrophic coculture of anaerobic bacteria. *Science.* **330**: 1413–5.

Sun, Q., Xiao, W., Xi, D., Shi, J., Yan, X., and Zhou, Z. (2010) Statistical optimization of biohydrogen production from sucrose by a co-culture of *Clostridium acidisoli* and *Rhodobacter sphaeroides*. *Int. J. Hydrogen Energy* **35**: 4076–4084.

Thomason, L.C., Costantino, N., and Court, D.L. (2007) *E. coli* genome manipulation by P1 transduction. *Curr. Protoc. Mol. Biol.* 1.17.1-1.17.8.

Wanner, U. and Egli, T. (1990) Dynamics of microbial growth and cell composition in batch culture. *FEMS Microbiol. Rev.* **6**: 19–43.

Widder, S., Allen, R.J., Pfeiffer, T., Curtis, T.P., Wiuf, C., Sloan, W.T., et al. (2016) Challenges in microbial ecology: building predictive understanding of community function and dynamics. *ISME J.* **10**: 2557-2568.

Figure Legends

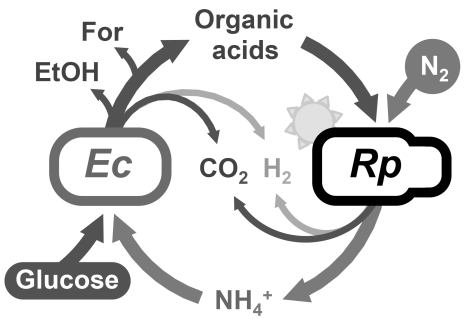

Fig. 1. Bi-directional anaerobic cross-feeding between fermentative *E. coli* and phototrophic *R. palustris* Nx. *E. coli* anaerobically ferments glucose into fermentation products, including the organic acids acetate, lactate, and succinate, which provide essential carbon for *R. palustris* Nx. In return *R. palustris* Nx uses light energy to fix N_2 and excrete NH_4^+, which provides *E. coli* with essential nitrogen. Formate and ethanol, produced by *E. coli*, and CO_2 and H_2, produced by both species, accumulate. *E. coli* fermentation can be growth-independent. Filled bubbles indicate compounds externally added to the coculture.

Fig. 2. Limiting N_2 in monoculture results in decreased NH_4^+ excretion. Final cell densities (A) and supernatant NH_4^+ levels (**B**) in stationary-phase *R. palustris* CGA4004 (Parent) and CGA4005 (Nx) monocultures. *R. palustris* was cultured in MDC with 5 mM acetate, with a headspace of 100% N_2 or 18% N_2, and incubated either horizontally with shaking or upright without agitation (static). Error bars indicate SD, n=3-6. Different letters indicate statistical differences, $p < 0.0001$, determined by one-way ANOVA (DFn, DFd = 4, 16; (**A**) F = 50; (**B**) F= 269) with Tukey's multiple comparisons post test.

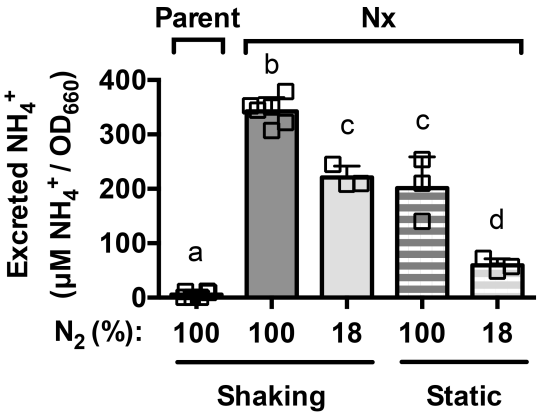

Fig. 3. Cocultures maintain coexistence despite lower NH_4^+ cross-feeding. H_2 yields (**A**) and normalized growth rates (**B**) of cocultures grown with various N_2 concentrations (% of gas in 17 ml of headspace) under shaking conditions. Circles indicate empirical data. Lines indicate SyFFoN_v2 model predictions. (**A**) Shaded region indicates low N_2 concentrations where empirical trends do not match model predictions. (**B**) Empirical and simulated growth rates are normalized to the corresponding average measured or simulated growth rate of cocultures with 100% N_2 (parameter N = 70 mM).

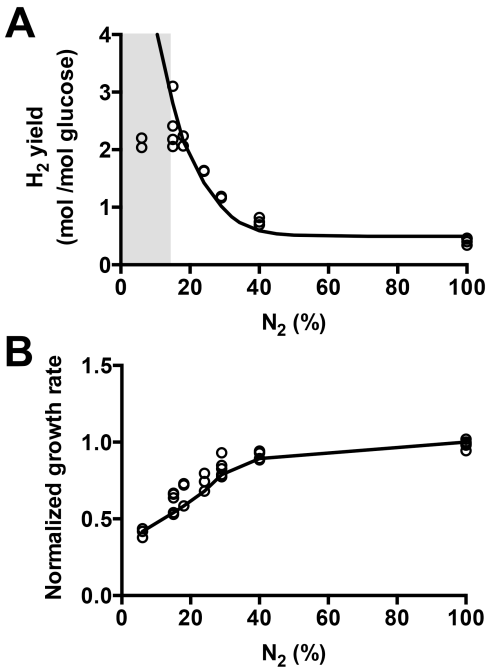

Fig. 4. N_2-limited cocultures exhibit stable coexistence and reproducible trends through serial transfers in a well-mixed environment. Species growth yields and final *E. coli* percentages (**A**), H_2 yields (**B**), and growth rates (**C**) from three serial transfers of shaken cocultures grown with 18% N_2. Transfer 1 was inoculated from a stationary phase starter coculture grown under 100% N_2 with shaking. Cocultures were serially transferred every 7 days. Error bars indicate 95% CI, n=4. Shaded horizontal bars indicate 95% CI for shaken cocultures grown with 100% N_2 (LaSarre *et al.*, 2017). (**A**) Growth yields are compared for each species rather than final cell densities to account for incomplete glucose consumption after 1 week in cocultures with 18% N_2. Final *E. coli* (*Ec*) percentages are the mean ± SD, n=4. *, statistical difference from *E. coli* percentages in shaken cocultures serially transferred with 100% N_2 (LaSarre *et al.*, 2017), $p < 0.001$, determined using one-way ANOVA (DFn, DFd = 3, 12; F = 13) with Tukey's multiple comparison post test.

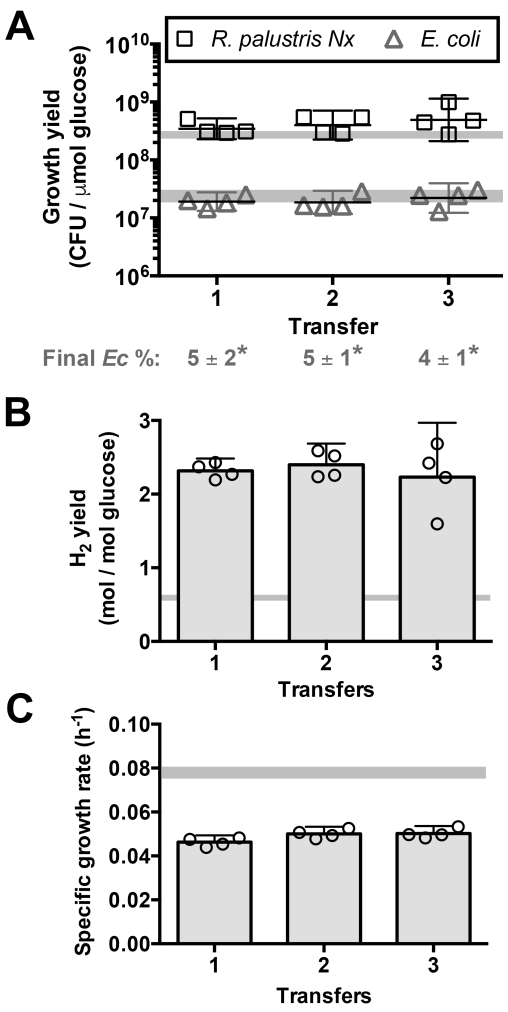

Fig. 5. N_2-limited cocultures exhibit stable coexistence and reproducible trends through serial transfers in a heterogeneous environment. H_2 yields (**A**), and individual species growth yields and final *E. coli* percentages (**B**) from three serial transfers of static cocultures grown with either 100% or 18% N_2. Transfer 1 was inoculated from a stationary phase starter coculture grown under 100% N_2 with shaking. Static cocultures with 100% N_2 and 18% N_2 were serially transferred every 2 and 4 weeks, respectively. Error bars indicate 95% CI, n=4. Shaded horizontal bars indicate 95% CI for shaken cocultures grown with 100% N_2 (LaSarre *et al.*, 2017). (**A**) Different letters indicate statistical differences, $p < 0.01$, determined by one-way ANOVA (DFn, DFn = 5, 18; F = 7) with Tukey's multiple comparisons post test. (**B**) Final *E. coli* (*Ec*) percentages are the mean ± SD, n=4; *statistical difference from *E. coli* percentages in shaken cocultures serially transferred with 100% N_2 (LaSarre *et al.*, 2017), $p < 0.0001$, determined using one-way ANOVA (DFn, DFn = 3, 12; (100%) F = 34; (18%) F= 56) with Tukey's multiple comparison post test.

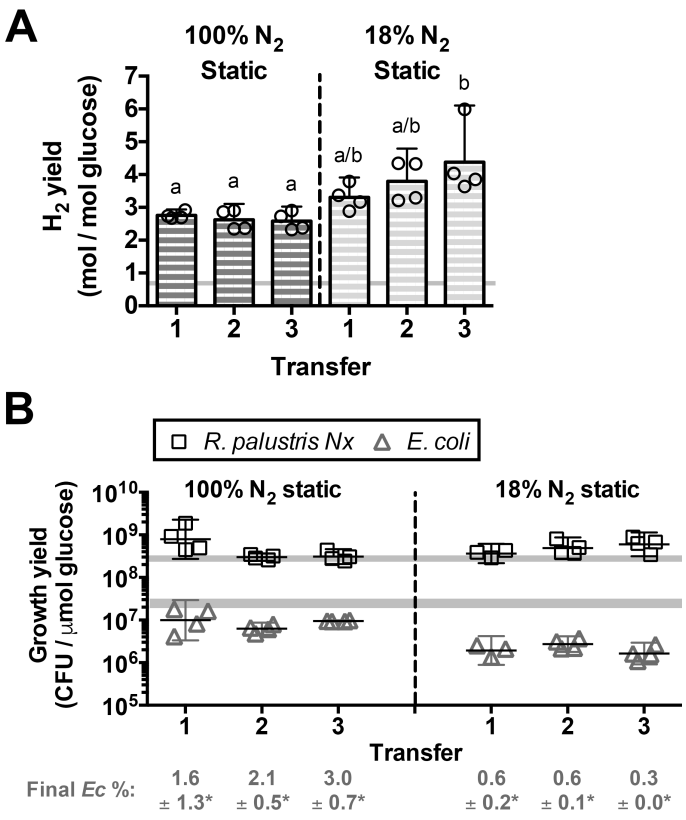

Fig. 6. Fermentative maintenance metabolism facilitates carbon cross-feeding. (A) Timecourse of *E. coli* ΔHisB and *R. palustris* cell densities and glucose consumption in coculture. *E. coli* ΔHisB and *R. palustris* were inoculated at equivalent CFUs/mL. Most error bars are too small to see. Error bars indicate SD, n=3. (**B**) Estimated carbon for glucose consumption, *E.* coli lysis, and *R. palustris* growth based on the data in (**A**). Conversion of CFU/ml to mM carbon is described in the Methods. Error bars indicate SD, n=3. Numerical values are averages ± SD.

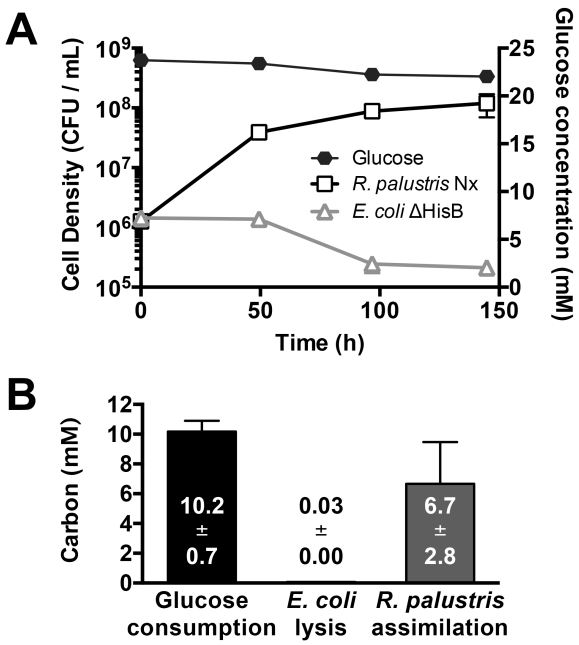

Fig. 7. Fermentative maintenance metabolism permits coexistence at low NH_4^+ cross-feeding levels. Simulated cell densities (lines) from cocultures grown with different N_2 concentrations when maintenance metabolism is included (**A**) or omitted (**B**) from the model. $Ec_{i\,sim}$ and $Rp_{i\,sim}$, initial simulated *E. coli* (*Ec*) and *R. palustris* (*Rp*) cell densities; $Ec_{f\,sim}$ and $Rp_{f\,sim}$, final simulated *E. coli* and *R. palustris* cell densities. Symbols are empirical CFU/mL data for *E. coli* ($Ec_{f\,emp}$) and *R. palustris* ($Rp_{f\,emp}$) from 7 day samples from shaken cocultures with 6%, 18%, 40% or 100% N_2. The same empirical data is overlaid on both panels (n=3).

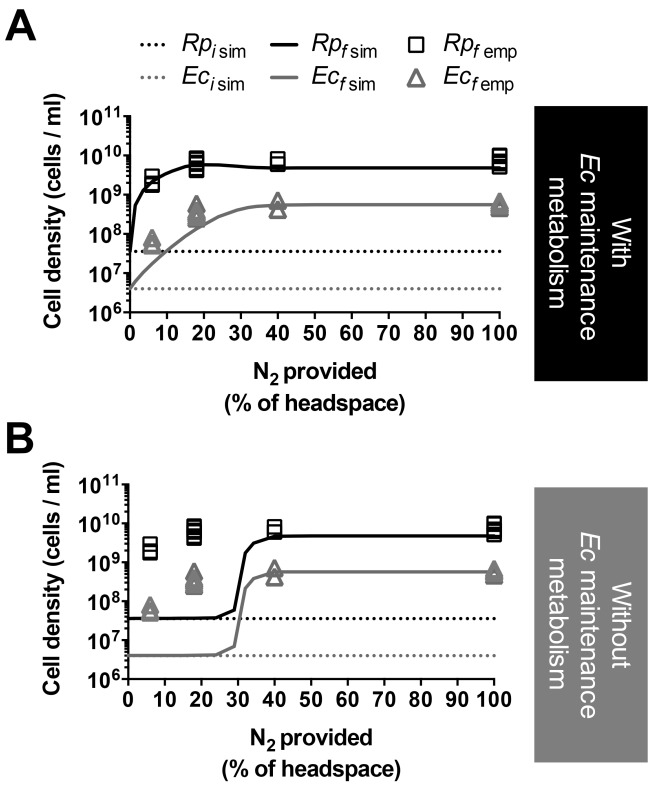

Figure 8. Fermentative maintenance metabolism prevents coculture growth at high *E. coli* cell densities. (**A-C**) Simulated changes in *E. coli* (Ec_{sim}) and *R. palustris* (Rp_{sim}) cell densities (lines) in cocultures grown with 100% N_2 with different initial *E. coli* cell densities when maintenance metabolism is included (**A, C**) or omitted (**B**) from the model. The simulated initial *R. palustris* cell density was 10^7 cells/ml. (**A, C**) These two simulations were identical except that (**C**) included initial consumable organic acids [C] and formate [f] levels that were calculated by multiplying the initial *E. coli* cell density by the 0 – 1 day maintenance fermentation rate shown in Supporting Information Fig. S9 x 24 h. Symbols are empirical CFU/mL data for *E. coli* (Ec_{emp}) and *R. palustris* (Rp_{emp}) from cocultures with different initial *E. coli* cell densities and an average initial *R. palustris* density of 2.4 x 10^7 ± 0.3 x 10^7 CFU/ml. Experimental cell densities were determined 10 d after coculture inoculation. The measured coculture pH after 10 d is also shown. (**D**) Simulated *E. coli* and *R. palustris* growth when cocultures grown with 100% N_2 are initiated from different initial cell densities. Species ratios are shown under the cell densities.

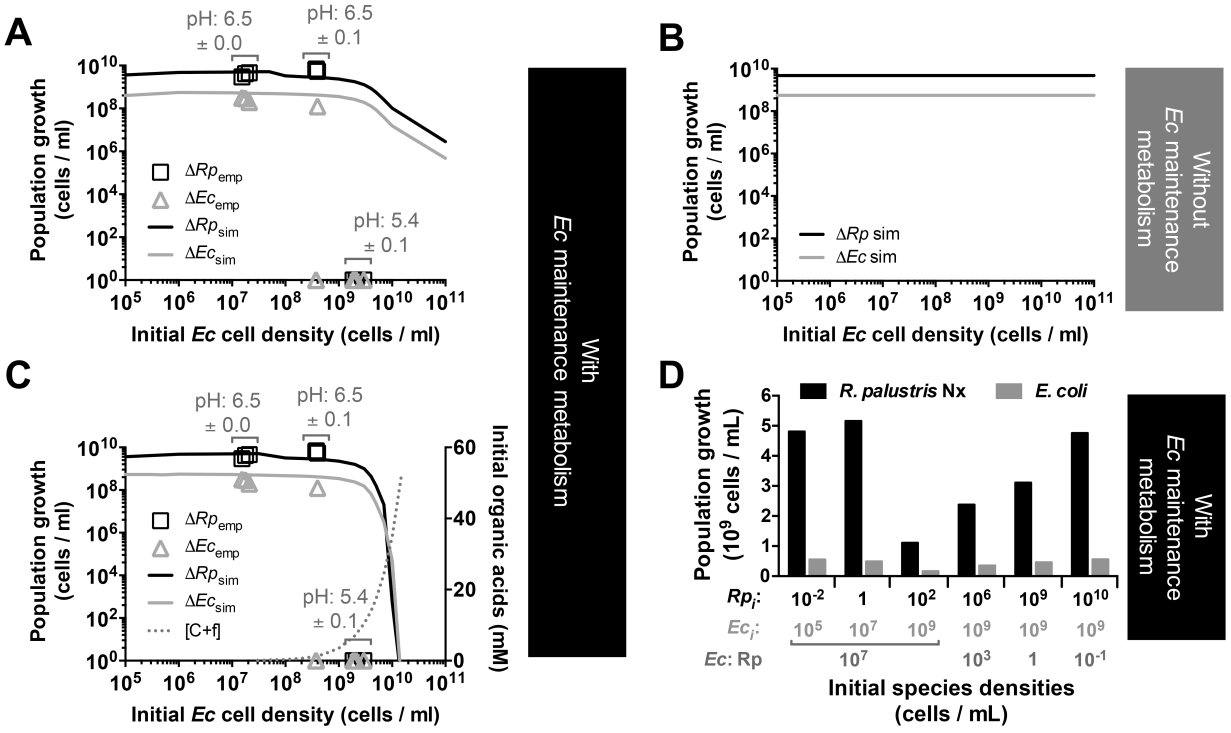

Supporting Information

Growth-independent cross-feeding modifies boundaries for coexistence in a bacterial mutualism

Alexandra L. McCully, Breah LaSarre, and James B. McKinlay
Department of Biology, Indiana University, Bloomington, IN

Methods

Mathematical modeling. A Monod model describing bi-directional cross-feeding in batch cultures, called SyFFoN_v2 (Syntrophy between Fermenter and Fixer of Nitrogen), was modified from our previous model (LaSarre *et al.*, 2017) as follows: (i) a sigmoidal function, rather than a Monod function, was used to control the transition to growth-independent fermentation ($10/(10+1.09^{(1000*uEc)})$); (ii) sigmoidal functions were used to transition from NH_4^+ excretion ($1-(40/(40+1.29^N))$) to H_2 production ($40/(40+1.29^N)$) by *R. palustris* as N_2 becomes limiting; (iii) a sigmoidal function was used to simulate the inhibiting effects of accumulated organic acids on both growth and metabolism for both species ($b_x/(b_x+10^{(f+C)})$); (iv) a sigmoidal function was used to dampen growth-independent fermentation rates when consumable organic acids (lactate, succinate, and acetate) accumulate ($r_x*(100/(100+6^C)) + r_x\_mono$) and simulate the slow growth-independent fermentation observed in *E. coli* monocultures (LaSarre *et al.*, 2017), compared to faster growth-independent fermentation in coculture; (v) *R. palustris* H_2 production was coupled to consumable organic acid depletion, assuming that 0.5 CO_2 are produced per H_2 (McKinlay *et al.*, 2014); (vi) the *R. palustris* Km for N_2 (K_N) was given a value of 6 mM, based on the change in growth rate at limiting N_2 concentrations in coculture; (vii) product formation parameters (R and r) were increased to more accurately simulate observed growth rates in coculture; (viii) the *E. coli* acid resistance parameter (b_{Ec}) was increased relative to that for *R. palustris* (b_{Rp}) based on terminal pH values observed in *E. coli* monocultures versus

cocultures. The effects of these modifications can be visualized in Figure S4. Equations are listed below with default values in Supplementary Table 2. SyFFoN_v2 runs in R studio and is available for download at: https://github.com/McKinlab/Coculture-Mutualism.

Equations 1 and 2 were used to describe *E. coli* and *R. palustris* growth rates:

Eq. 1: *E. coli* growth rate; $\boldsymbol{\mu_{Ec}} = \mu_{EcMAX} \bullet [G/(K_G+G)] \bullet [A/(K_A+A)] \bullet [b_{Ec}/(b_{Ec}+10^{(f+C)})]$

Eq. 2: *R. palustris* growth rate; $\boldsymbol{\mu_{Rp}} = \mu_{RpMAX} \bullet [C/(K_C+C)] \bullet [N/(K_N+N)] \bullet [b_{Rp}/(b_{Rp}+10^{(f+C)})]$

Equations 3-12 were used to describe temporal changes in cell densities and extracellular compounds. Numerical constants in product excretion equations are used to account for molar stoichiometric conversions. Numerical constants used in sigmoidal functions are based on those values that resulted in simulations resembling empirical trends. All R and r parameters are expressed in terms of glucose consumed except for $R_{A,}$ which is the amount of NH_4^+ produced per *R. palustris* cell (Supplementary Table 2).

Eq. 3: Glucose; $\boldsymbol{dG/dt} = -\mu_{Ec} \bullet Ec/Y_G - \mu_{Ec} \bullet Ec \bullet (R_c+R_f+R_e+R_{CO2}) -$

$Ec \bullet (G/(K_G+G)) \bullet (10/(10+1.09^{(1000 \bullet \mu Ec)})) \bullet (b_{Ec}/(b_{Ec}+10^{(f+C)})) \bullet ((100/(100+6^C)) \bullet$

$(r_C+r_f+r_e+r_{CO2}) + r_{C\_mono} + r_{f\_mono} + r_{e\_mono} + r_{CO2\_mono})$

Eq. 4: N_2; $\boldsymbol{dN/dt} = -\mu_{Rp} \bullet Rp \bullet 0.5 \bullet R_A \bullet (1-(40/(40+1.29^N)) - \mu_{Rp} \bullet Rp/Y_N$

Eq. 5: Consumable organic acids; $\boldsymbol{dC/dt} = Ec \bullet 2 \bullet (\mu_{Ec} \bullet R_c +$

$(G/(K_G+G)) \bullet (10/(10+1.09^{(1000 \bullet \mu Ec)})) \bullet (b_{Ec}/(b_{Ec}+10^{(f+C)})) \bullet (r_C \bullet (100/(100+6^C)) + r_{C\_mono})) -$

$(\mu_{Rp} \bullet Rp/Y_C) - 0.25 \bullet Rp \bullet (\mu_{Rp} \bullet Rh_{Rp} + r_{Hp} \bullet (C/(K_C+C)) \bullet (40/(40+1.29^N)) \bullet (b_{Rp}/(b_{Rp}+10^{(f+C)})))$

Eq. 6: Formate; $\boldsymbol{df/dt} = Ec \bullet 6 \bullet (\mu_{Ec} \bullet R_f + (G/(K_G+G)) \bullet (10/(10+1.09^{(1000 \bullet \mu Ec)})) \bullet$

$(b_{Ec}/(b_{Ec}+10^{(f+C)})) \bullet (r_f \bullet (100/(100+6^C)) + r_{f\_mono}))$

Eq. 7: NH_4^+; $\boldsymbol{dA/dt} = Rp \bullet \mu_{Rp} \bullet R_A \bullet (1-(40/(40+1.29^N))) - \mu_{Ec} \bullet Ec/Y_A$

Eq. 8: *E. coli*; $\boldsymbol{dEc/dt} = \mu_{Ec} \bullet Ec$

Eq. 9: *R. palustris*; $\boldsymbol{dRp/dt} = \mu_{Rp} \bullet Rp$

Eq. 10: Ethanol; $\boldsymbol{de/dt} = Ec \bullet 3 \bullet (\mu_{Ec} \bullet R_e + (G/(K_G+G)) \bullet (10/(10+1.09^{(1000 \bullet \mu Ec)}))$

$\bullet (b_{Ec}/(b_{Ec}+10^{(f+C)})) \bullet (r_e \bullet (100/(100+6^C)) + r_{e\_mono}))$

Eq. 11: CO_2; $\boldsymbol{dCO2/dt} = Ec \bullet 6 \bullet (\mu_{Ec} \bullet R_{CO2} + (G/(K_G+G)) \bullet (10/(10+1.09^{(1000 \bullet \mu Ec)})) \bullet$

$(b_{Ec}/(b_{Ec}+10^{(f+C)})) \bullet (r_{co2} \bullet (100/(100+6^C)) + r_{co2\_mono})) + Rp \bullet 0.5 \bullet (\mu_{Rp} \bullet Rh_{Rp} +$

$r_{Hp} \bullet (C/(K_C+C)) \bullet (40/(40+1.29^N)) \bullet (b_{Rp}/(b_{Rp}+10^{(f+C)})))$

Eq. 12: H_2; $\boldsymbol{dH/dt} = Rp \bullet (\mu_{Rp} \bullet R_{HRp} + r_{Hp} \bullet (C/(K_C+C)) \bullet (40/(40+1.29^N)) \bullet$

$(b_{Rp}/(b_{Rp}+10^{(f+C)}))) + Ec \bullet (\mu_{Ec} \bullet R_{HEc} + (G/(K_G+G)) \bullet (10/(10+1.09^{(1000 \bullet \mu Ec)})) \bullet$

$(b_{Ec}/(b_{Ec}+10^{(f+C)})) \bullet (r_H \bullet (100/(100+6^C)) + r_{H\_mono}))$

Where,

μ is the specific growth rate of the indicated species (h^{-1}).

μ_{MAX} is the maximum specific growth rate of the indicated species (h^{-1}).

G, A, C, N, f, e, H and CO2 are the concentrations (mM) of glucose, NH_4^+, consumable organic acids, N_2, formate, ethanol, H_2, and CO_2, respectively. All gasses are assumed to be fully dissolved. Consumable organic acids are those that *R. palustris* can consume, namely, lactate (3 carbons), acetate (2 carbons), and succinate (4 carbons). All consumable organic acids were simulated to have three carbons for convenience. Only net accumulation of formate, ethanol, CO_2 and H_2 are described in accordance with observed trends.

K is the half saturation constant for the indicated substrate (mM).

Ec and Rp are the cell densities (cells/ml) of *E. coli* and *R. palustris*, respectively.

b is the ability of a species to resist the inhibiting effects of acid (mM). Default values were chosen based on levels of formate and other organic acids observed to inhibit growth and metabolism in cocultures and *E. coli* monocultures.

Y is the *E. coli* or *R. palustris* cell yield from the indicated substrate (cells / μmol glucose). Y values were determined in MDC with the indicated substrate as the limiting nutrient.

R is the fraction of glucose converted into the indicated compound per *E. coli* cell during growth (μmol of glucose / *E. coli* cell), except for R_A. Values were adjusted to accurately simulate product yields measured in cocultures and in MDC with and without added NH_4Cl.

R_A is the ratio of NH_4^+ produced per *R. palustris* cell during growth (μmol / *R. palustris* cell). The default value was based on that which accurately simulated empirical trends.

r is the growth-independent rate of glucose converted into the indicated compound (μmol / cell / h). Default values are based on those which accurately simulated empirical trends in coculture.

$r_{\_mono}$ is the growth-independent rate of glucose converted into the indicated compound by *E. coli* when consumable organic acids accumulate. Default values are based on linear regression of products accumulated over time in nitrogen-free cell suspensions of *E. coli* (LaSarre *et al.*, 2017).

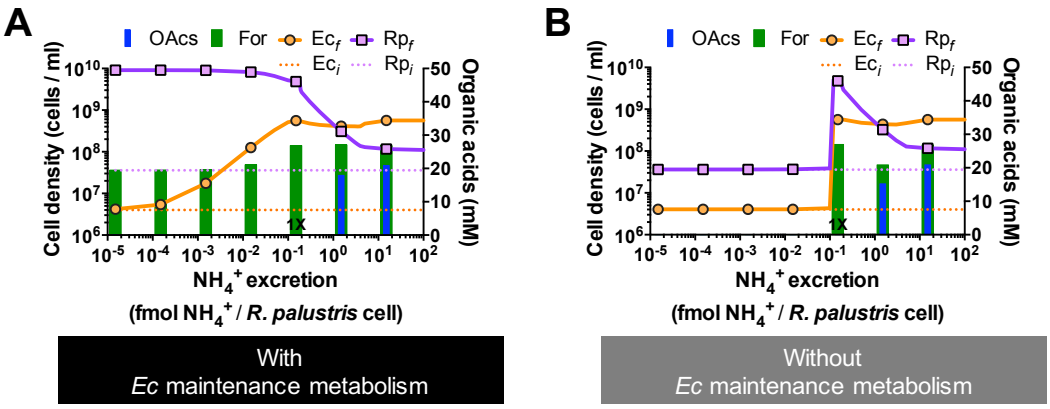

Figure S1. SyFFoN_v2 predicts that coexistence at low NH_4^+ cross-feeding levels requires *E. coli* maintenance metabolism. Simulated effect of the *R. palustris* NH_4^+ excretion level on growth and organic acid accumulation in 100% N_2-supplied cocultures in the presence (**A**) or absence (**B**) of *E. coli* maintenance metabolism. 1X is the default NH_4^+ excretion level (0.15 fmol NH_4^+ / cell) and is thought to represent that excreted by *R. palustris* Nx based on model approximation of empirical trends. OAcs, consumable organic acids (lactate, acetate, and succinate); For, formate; Ec_i and Rp_i, initial *E. coli* (*Ec*) and *R. palustris* (*Rp*) cell densities; Ec_f and Rp_f, final *E. coli* and *R. palustris* cell densities. (**A**) Trends from SyFFoN_v2 are consistent with trends from a previous version of the model (LaSarre *et al.*, 2017).

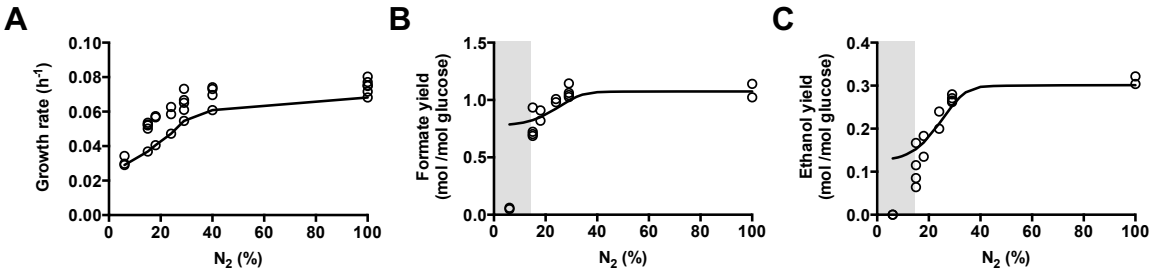

Figure S2. SyFFoN_v2 predictions of growth rates (A), formate yields (B), and ethanol yields (C) at various N_2 concentrations. Circles indicate empirical data from shaken cocultures. Lines indicate model predictions. Shaded regions indicate low N_2 concentrations where empirical trends do not match model predictions.

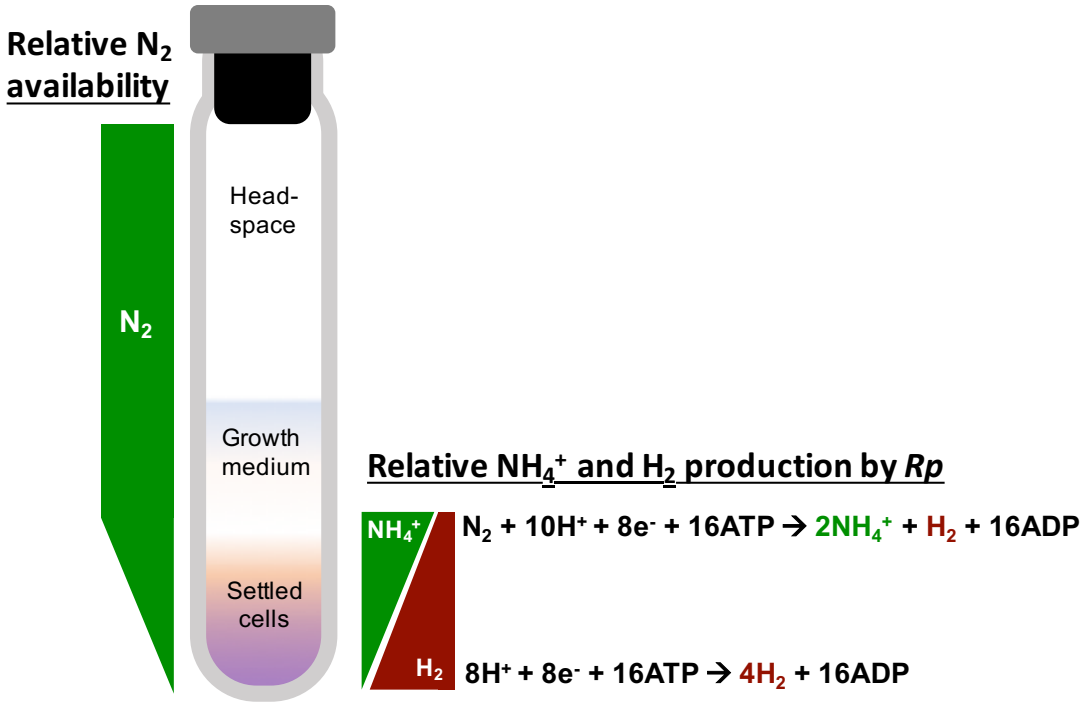

Figure S3. Cell settling in static cocultures is assumed to lead to zone of N_2 limitation that favors H_2 production over NH_4^+ production. With saturating N_2, nitrogenase produces 2 moles of NH_4^+ and one mole of H_2 for every mole of N_2 fixed (top equation). When N_2 is absent, nitrogenase only produces H_2 (bottom equation). Under sub-saturating N_2 conditions, the amounts of NH_4^+ and H_2 produced would be somewhere between the two equations.

A

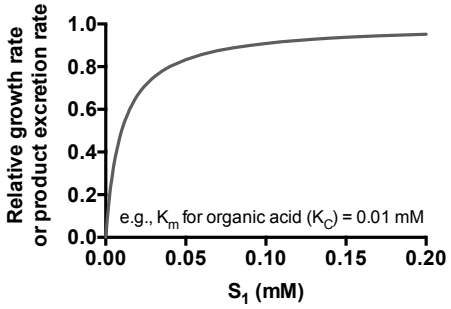

$\mu_X = \mu_X Max \bullet \ldots \bullet \mathbf{S1/(K_{S1}+S1)}$

Where,
μ_X is the growth rate of species X (h^{-1})
$\mu_X Max$ is the maximum growth rate of speceis X (h^{-1})
$S_\#$ is the concentration of a given substrate (mM)
$K_{S\#}$ is the Km value for a given substrate (mM)

B

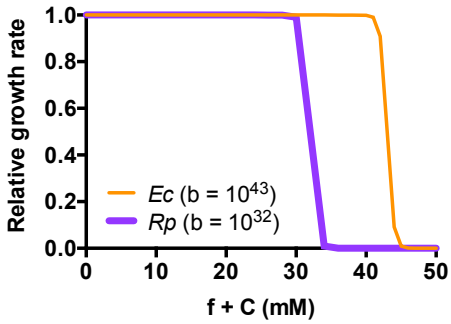

$\mu_X = \mu_X Max \bullet \mathbf{\ldots \bullet b_X/(b_X+10^{(f+C)})}$

Where,
μ_X is the growth rate of species X (h^{-1})
$\mu_X Max$ is the maximum growth rate of speceis X (h^{-1})
b_X is an arbitrary value used to indicate the ability of species X to resist inhibition by acid
f is the concentration of formate (mM)
C is the concentration of consumable organic acids (acetate, lactate, and succinate; mM)

C

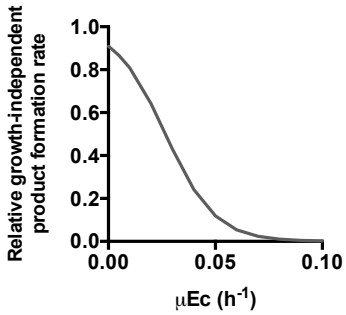

$dP/dt = r_P \bullet \ldots \bullet \mathbf{10/(10+1.09^{(1000 \bullet \mu Ec)})}$

Where,
dP/dt is the change in product concentration per unit time (mM/h)
r_P is the maximum growth-independent rate of product formation in coculture
μEc is the growth rate of *E. coli* (h^{-1})

D

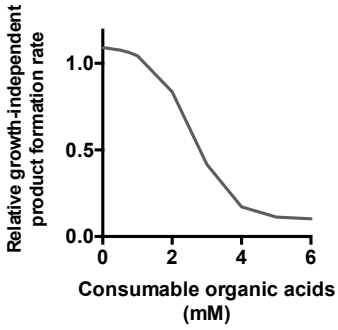

$dP/dt = r_P \bullet \ldots \bullet \mathbf{(100/(100+6^C)+r_{P\_mono})}$

Where,
dP/dt is the change in product concentration per unit time (mM/h)
r_P is the maximum growth-independent rate of product formation in coculture
r_P is the maximum growth-independent rate of product formation in coculture
r_{P_mono} is the maximum growth-independent rate of product formation in *E. coli* cell suspensions

E

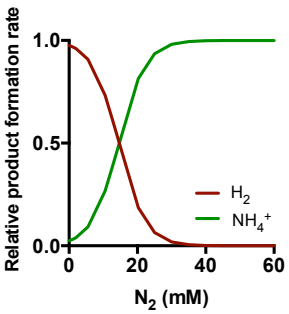

$dA/dt = Rp \bullet \mu Rp \bullet RA \bullet \ldots \bullet \mathbf{1 - (40/(40+1.29^N))}$
$dH/dt = rHp \bullet \ldots \bullet \mathbf{40/(40+1.29^N)}$

Where,
dP/dt is the change in product concentration per unit time (mM/h)
r_P is the maximum growth-independent rate of product formation in coculture
r_P is the maximum growth-independent rate of product formation in coculture
r_{P_mono} is the maximum growth-independent rate of product formation in *E. coli* cell suspensions

Figure S4. The effect of SyFFoN_v2 functions on growth rate and product formation rates. **(A)** Growth rate approaches zero as substrate supply is exhausted according to a Monod model (whole-cell Michaelis-Menten kinetics). The function, $S1/(K_{S1}+S1)$, is used in SyFFoN_v2 equations 1 and 2 to control growth rates in response to substrate concentration. The function was also used in equations 3, 5, 6, 10, 11, and 12 to control growth-independent product excretion rates in response to substrate concentration. The function was not applied to growth-dependent product excretion rates since these are already dependent on growth rate which in turn is dependent on substrate concentration. Km values were taken from the literature or assumed as indicated in Supplementary Table 2. The Km value for N_2 was determined experimentally from *R. palustris* exponential growth rates at different N_2 concentrations (Figure S5).

(B) Growth rate declines sharply at a threshold organic acid concentration according to the sigmoidal function, $b_X/(b_X+10^{(f+C)})$. The curve was modeled to resemble that of an acid titration curve in buffer. The function is used in equations 1 and 2 to control growth rate in response to acid accumulation. The function was also used in equations 3, 5, 6, 10, 11, and 12 to control growth-independent product excretion rates in response to acid accumulation. The function was not applied to growth-dependent product excretion rates since these are already dependent on growth rate which in turn is dependent on organic acid concentration. Values for 'b' were determined by manually varying values until simulated growth inhibition occurred at organic acid levels resembling those observed in cocultures and *E. coli* monocultures with excess glucose, such that growth halted due to acid accumulation.

(C) *E. coli* growth-independent fermentation rates (μmol / cell / h) increase as the *E. coli* growth rate decreases according to the sigmoidal function, $10/(10+1.09^{(1000 \cdot \mu Ec)})$. The function is used in equations 3, 5, 6, 10, 11, and 12 to transition to growth-independent product formation rates when *E. coli* growth slows. Product formation rates associated with maintenance metabolism (r) were modeled to increase as *E. coli* growth slows rather than being kept constant since product formation rates observed in non-growing *E. coli* cell suspensions with glucose could not explain the rate of *R. palustris* growth and formate accumulation in cocultures. Consumption of organic acids by *R. palustris* likely increases these growth-independent fermentation rates by removing inhibitory effects of end-products. The values of '10' and '1.09' were arrived at after manually trying several arbitrary values to control the total time for coculture growth (see Figure S6A).

(D) *E. coli* growth-dependent fermentation rates (μmol / cell / h) decrease to a rate observed in non-growing *E. coli* cell suspensions as consumable organic acid concentrations increase according to the sigmoidal function, $(100/(100+6^{C}))+r_{P\_mono}$. The function is used in equations 3, 5, 6, 10, 11, and 12 to transition to growth-independent product formation rates observed in *E. coli* cell suspensions when consumable organic acids accumulate. This function is necessary to ensure that the model does not use the high growth-independent fermentation rates observed in coculture when consumable organic acids accumulate (e.g., when the NH_4^+ availability is low and the *E. coli* density is high, or in nitrogen-starved *E. coli* cell suspensions). The function uses C (consumable organic acids) instead of (C+f) (consumable organic acids and formate), to avoid incorrectly halting formate production in cocultures even when C is fully consumed. The values of '100' and '6' were arrived at after manually trying several arbitrary values to control the levels of organic acid accumulation similar to what is observed in nitrogen-starved *E. coli* cell suspensions (see Figure S6B and C).

(E) As N_2 availability increases, the *R. palustris* nitrogenase activity shifts from producing only H_2 to a mixture of H_2 and NH_4^+ according to:

No N_2: $8H^+ + 8e^- + 16\ ATP \rightarrow 4H_2 + 16\ ADP$

Saturating N_2: $N_2 + 10H^+ + 8e^- + 16\ ATP \rightarrow 2NH_4^+ + H_2 + 16\ ADP$

In SyFFoN_v2 this shift is controlled by two functions. One function, **1-(40/(40+1.29^N))** (green) is used in equation 4 to increase NH_4^+ production with increasing N_2 concentration. The other function, **40/(40+1.29^N)** (red) is used in equation 12 to decrease H_2 production with increasing N_2 concentration. The values of '40' and '1.29' were arrived at after manually trying several arbitrary values to control the shape of the curves and give final product yields similar to those observed in Figure 3 and Figure S2 (see also Figure S6D).

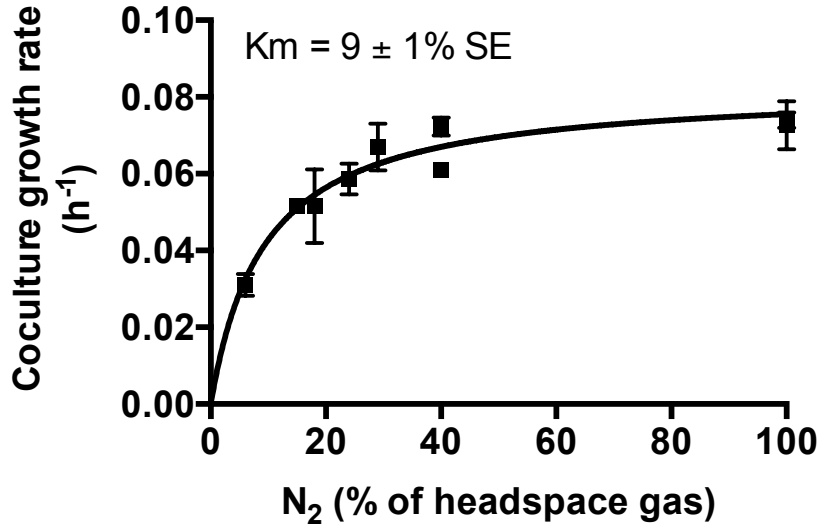

Figure S5. Determination of *R. palustris* whole cell Km value for N_2 in coculture. A Michaelis-Menten curve was fit to coculture growth rate data determined at various N_2 concentrations using Graphpad Prism v.6.0h. Symbol error bars are SD.

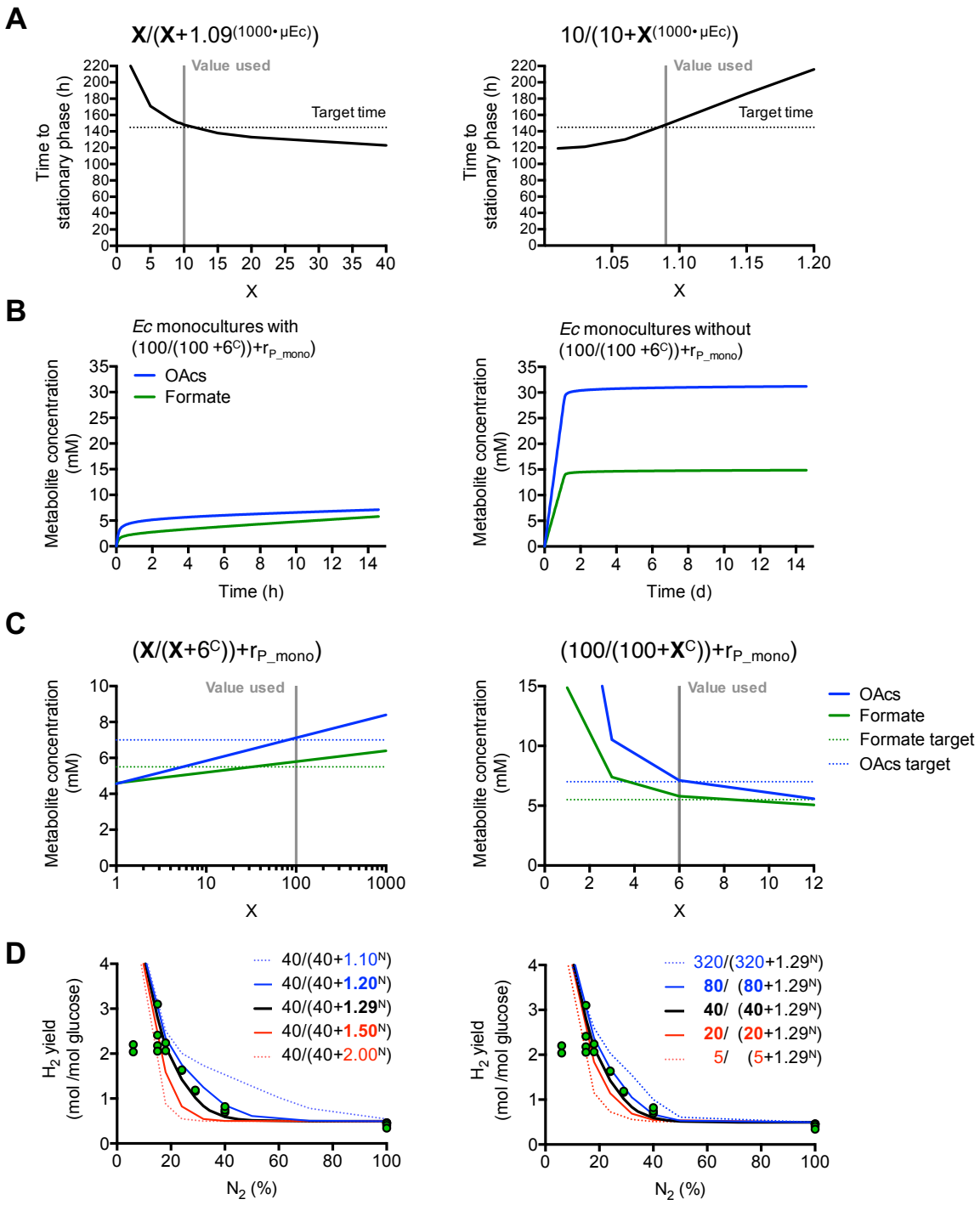

Figure S6. Effect of arbitrarily chosen function values on simulated trends.
(A) Altering the arbitrary values of 10 (left panel) and 1.09 (right panel) in the function **10/(10+1.09$^{(1000\bullet\ \mu Ec)}$)** affects the simulated time required for cocultures to reach stationary phase (i.e., when the optical density is observed to plateau). The example shown is for simulated coculture times with 18% N_2 for which experimental cocultures were observed to reach stationary phase in approximately 145 h (dotted line).

(B) The function **$(100/(100+6^{C}))+r_{P\_mono}$)** is necessary to dampen product excretion rates associated with *E. coli* maintenance metabolism (r) when consumable organic acids accumulate, such as in simulations of nitrogen-starved *E. coli* cell suspensions (left panel; compare with trends in Figure S9) or when *E. coli* cell densities in coculture are high but NH_4^+ availability is low. Without this function organic acids would accumulate in simulations of nitrogen-starved *E. coli* cell suspensions at an unrealistically high rate (right panel).

(C) Altering the arbitrary values of 100 (left panel) and 6 (right panel) in the function **$(100/(100+6^{C}))+r_{P\_mono}$)** affects the levels of metabolite accumulation in nitrogen-starved *E. coli* cell suspensions by 14 d. Target concentrations of 7 mM consumable organic acids and 5.5 mM formate were chosen based on approximate levels observed in experimental nitrogen-starved *E. coli* cell suspensions at 14 d (Figure S9).

(D) Altering the arbitrary values of 1.29 (left panel) and 40 (right panel) in the function **$40/(40+1.29^{N})$** affects product yields over different N_2 concentrations. The example shown overlays simulated H_2 yields (red and blue lines) on Figure 3A when different arbitrary values are used, with green dots representing experimentally determined H_2 yields and the black line representing simulated values when the values 40 and 1.29 were used in the function. Use of different arbitrary values similarly affected other simulated product yields and growth yields by shifting trends for away from observed values.

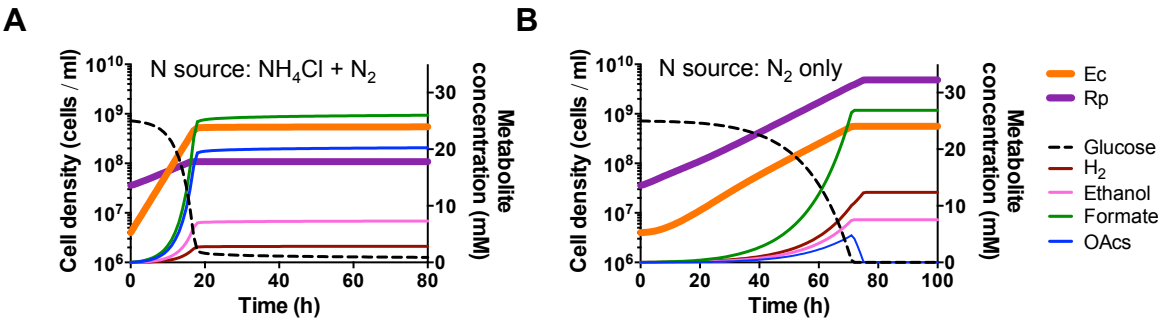

Figure S7. SyFFoN_v2 simulations of batch cocultures with and without externally added NH_4^+. (**A**, **B**) Simulated growth and metabolic profiles of cocultures supplied with NH_4^+ (parameter A = 15mM) (**A**) or 100% N_2 alone (**B**). *Ec*, *E. coli*; *Rp*, *R. palustris*; OAcs, consumable organic acids (lactate, acetate, and succinate). Trends from SyFFoN_v2 are consistent with trends from a previous version of the model (LaSarre *et al.*, 2017).

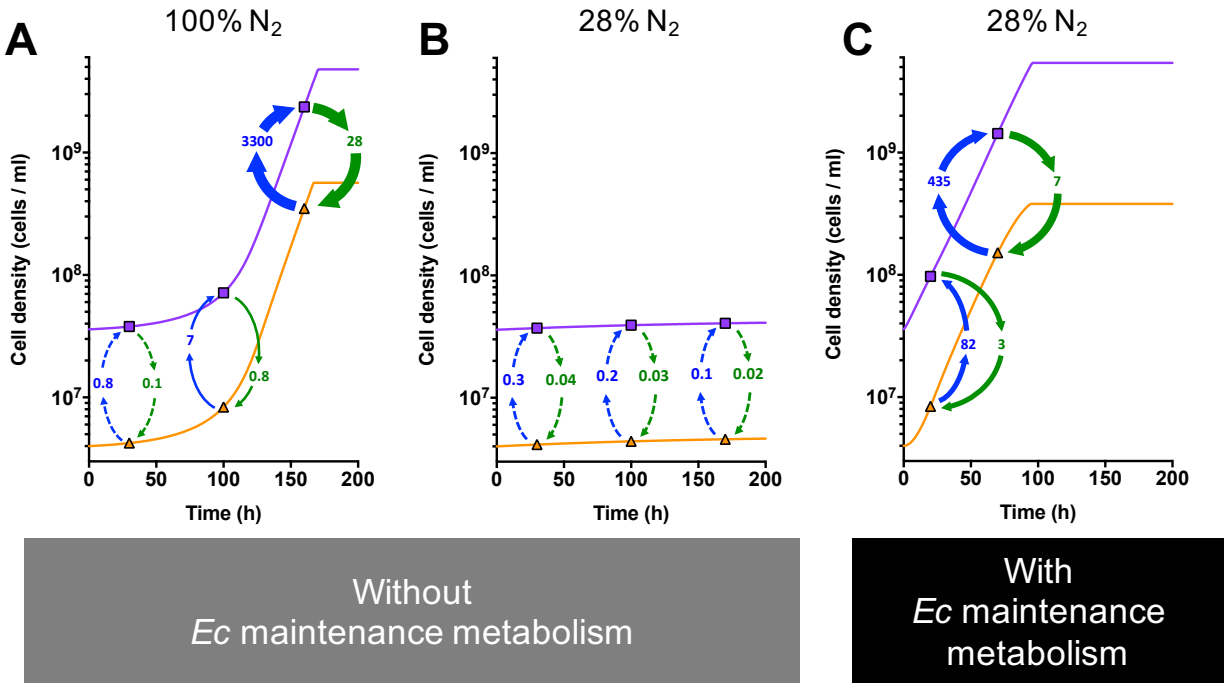

Figure S8. *E. coli* maintenance metabolism is predicted to permit coculture growth at low N_2 concentrations by circumventing diminishing returns. Simulated exchange of NH_4^+ (green) and consumable organic acids (blue) during growth of *E. coli* (orange lines, triangles) and *R. palustris* (purple lines, squares) populations when maintenance metabolism is omitted (**A**, **B**) or included (**C**). Cross-fed NH_4^+ and organic acid values for the indicated time points (symbols) are the sum of those free in the medium plus those assimilated in the exchange (μM).

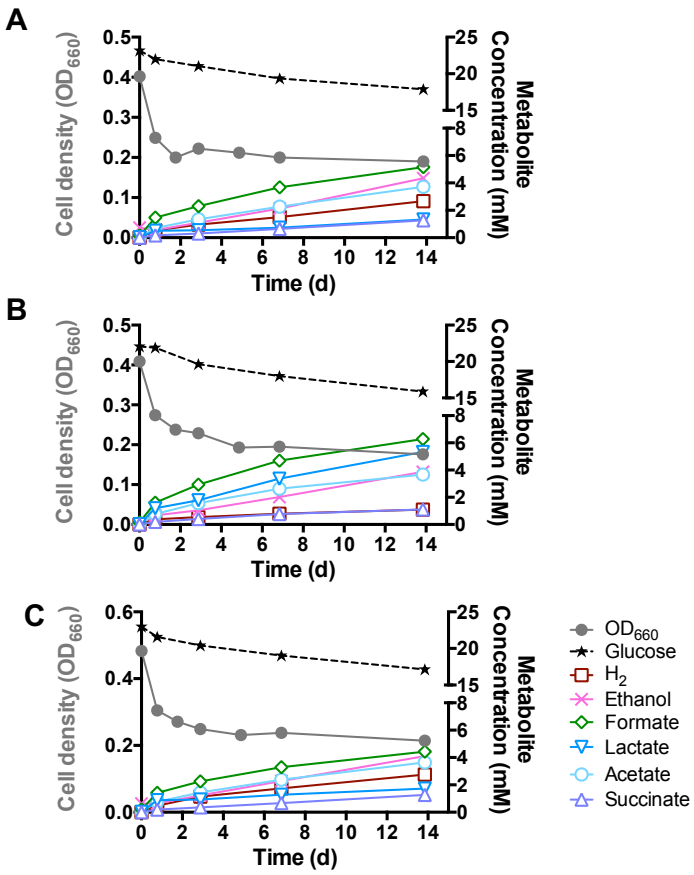

D

	Specific formation rate (attomol glucose / CFU / h)		Fold change
	0 – 1 days	1 – 7 days	
H_2	23 ± 5	7 ± 3	- 3.3
Ethanol	6 ± 5	5 ± 0	-1.2
Formate	11 ± 1	4 ± 1	-2.8
Lactate	21 ± 8	2 ± 0	-10.5
Acetate	12 ± 1	5 ± 1	-2.4
Succinate	6 ± 0	3 ± 1	-2.0

Figure S9. Estimation of *E. coli* fermentation rates associated with maintenance metabolism in cell suspensions lacking nitrogen. (A-C) Growth and metabolic trends in nitrogen-starved *E. coli* cell suspensions. Each panel is data from a separate biological replicate. **(D)** Average specific product formation rates (± SD) in *E. coli* cell suspensions for the indicated time frames, determined from the data in **A-C**. Fold changes in specific formation rates are shown for days 1 – 7 relative to days 0 – 1. Figure S8A is the same data that appeared in Supplementary Figure 1 in LaSarre *et al.,* 2017.

Table S1. Strains, plasmids and primers used in this study.

***R. palustris* strains;** designation in paper		
CGA009	Wild-type strain; spontaneous Cm^R derivative of CGA001	(Larimer *et al.*, 2004)
CGA4004	CGA009 Δ*hupS* Δ*rpa2750*; Parent	(LaSarre *et al.*, 2017)
CGA4005	CGA4004 *nifA**; Nx	(LaSarre *et al.*, 2017)
***E. coli* strains**		
MG1655	Wild-type K12 obtained from the Coli Genetic Stock Center (# 7740, MG1655(Seq)), WT	(Blattner *et al.*, 1997)
JW2004-1	*Δ(araD-araB)567, ΔlacZ4787(::rrnB-3), λ⁻, ΔhisB720::kan, rph-1, Δ(rhaD-rhaB)568, hsdR514*	(Baba *et al.*, 2006)
MG1655 ΔHisB	*MG1655 ΔhisB720::Km*	This study

Table S2. Default parameter values used in the model unless stated otherwise

Parameter	Value	Description (Units); Source
μ_{EcMAX}	0.2800	*E. coli* max growth rate (h^{-1}); Monoculture
μ_{RpMAX}	0.0772	*R. palustris* max growth rate (h^{-1}); Monoculture
G	25	Glucose (mM)
A	0.00005	NH_4^+ (mM); from initial $(NH_4)_6Mo_7O_{24}\cdot 4H_2O$ concentration
C	0	Consumable organic acids (those that *R. palustris* was observed to consun succinate; mM)
N	70	N_2 (assumed to be fully dissolved; mM)
f	0	Formate (mM)
e	0	Ethanol (mM)
CO2	0	Carbon dioxide (mM)
K_G	0.02	*E. coli* affinity (Michaelis-Menten constant (Km)) for glucose (mM); (Bul
K_C	0.01	*R. palustris* affinity (Km) for consumable organic acids (mM); Assumed
K_A	0.01	*E. coli* affinity for NH_4^+ (mM); (Khademi *et al.*, 2004)
K_N	6	*R. palustris* affinity (Km) for N_2 (mM); determined by fitting a Michaelis- of coculture growth rates versus N_2 concentration (Figure S5).
Ec	0.4×10^7	*E. coli* cell density (cells / ml)
Rp	3.6×10^7	*R. palustris* cell density (cells / ml)
b_{Ec}	10^{43}	Resistance of *E. coli* to low pH (mM)[a]
b_{Rp}	10^{32}	Resistance of *R. palustris* to low pH (mM)[a]
Y_G	8×10^7	Glucose-limited *E. coli* growth yield (cells / µmol glucose); Determined b by the concentration of glucose consumed at early stationary phase in gluc monocultures
Y_A	1×10^9	NH_4^+-limited *E. coli* growth yield (cells / µmol NH_4^+); Determined by div the concentration of NH_4^+ used at early stationary phase in NH_4^+-limited *E.*
Y_C	2.5×10^8	Organic acid-limited *R. palustris* growth yield (cells / µmol organic acid); dividing the CFU/ml by the concentration of acetate used at early stationary limited *R. palustris* monocultures
Y_N	5×10^8	N_2-limited *R. palustris* growth yield cells / µmol N_2; Determined by divin concentration of N_2 used at early stationary phase in N_2-limited *R. palustris*
R_C	1.9×10^{-8}	Fraction of glucose converted to organic acids (µmol glucose / cell)[a]
R_f	8×10^{-9}	Fraction of glucose converted to formate (µmol glucose / cell)[a]
R_e	4.5×10^{-9}	Fraction of glucose converted to ethanol (µmol glucose / cell)[a]
R_{CO2}	5×10^{-10}	Fraction of glucose converted to CO_2 (µmol glucose / cell)[a]
R_{HRp}	2×10^{-9}	*R. palustris* H_2 production (µmol H_2 / *R. palustris* cell)[a]
R_{HEc}	5×10^{-9}	*E. coli* H_2 production (µmol H_2 / *E. coli* cell) [a]
R_A	0.15×10^{-9}	*R. palustris* NH_4^+ production (µmol NH_4^+ / cell) [a]
r_C	300×10^{-11}	*E. coli* specific growth-independent rate of glucose conversion to consum (µmol glucose / cell / h)[a]
r_f	47×10^{-11}	*E. coli* specific growth-independent rate of glucose conversion to formate h)[a]
r_e	15×10^{-11}	*E. coli* specific growth-independent rate of glucose conversion to ethanol h)[a]

r_{CO2}	2×10^{-11}	*E. coli* specific growth-independent rate of glucose conversion to CO_2 (µn
r_H	2×10^{-11}	*E. coli* specific growth-independent rate of H_2 production (µmol H_2 / cell /
r_{C_mono}	1.2×10^{-11}	*E. coli* specific growth-independent rate of glucose conversion to consum when consumable organic acids accumulate (µmol glucose / cell / h)[b]
r_{f_mono}	0.83×10^{-11}	*E. coli* specific growth-independent rate of glucose conversion to formate organic acids accumulate (µmol glucose / cell / h)[b]
r_{e_mono}	0.5×10^{-11}	*E. coli* specific growth-independent rate of glucose conversion to ethanol organic acids accumulate (µmol glucose / cell / h)[b]
r_{co2_mono}	1.3×10^{-11}	*E. coli* specific growth-independent rate of glucose conversion to CO_2 wh acids accumulate (µmol glucose / cell / h)[b]
r_{H_mono}	0.83×10^{-11}	*E. coli* specific growth-independent rate of glucose conversion to H_2 when acids accumulate (µmol glucose / cell / h)[b]
r_{Hp}	27×10^{-11}	*R. palustris* specific growth-independent rate of H_2 production (µmol H_2 /

[a] Values were manually varied until simulated trends resembled empirical trends observed in both monoculture and coculture (i.e., growth inhibition at a given cumulative concentration of formate and other organic acids). Growth-independent fermentation rates were increased to account for *R. palustris*'s pull on *E. coli* metabolism by consuming organic acids.

[b] Determined from rates of product formation from glucose measured between days 1 and 7 of *E. coli* cell suspensions, wherein growth was prevented by omitting all nitrogen sources. Representative plots of fermentation product accumulation under these conditions is available in Figure S8.

Supplementary References

Baba, T., Ara, T., Hasegawa, M., Takai, Y., Okumura, Y., Baba, M., et al. (2006) Construction of *Escherichia coli* K-12 in-frame, single-gene knockout mutants: the Keio collection. *Mol. Syst. Biol.* **2**: 2006.0008.

Blattner, F., Plunkett G, I., Bloch, C., Perna, N., Burland, V., Riley, M., et al. (1997) The complete genome sequence of *Escherichia coli* K-12. *Science.* **2771613**: 1453–1462.

Buhr, A., Daniels, G.A., and Erni, B. (1992) The glucose transporter of *Escherichia coli*: Mutants with impaired translocation activity that retain phosphorylation activity. *J. Biol. Chem.* **267**: 3847–3851.

Khademi, S., O'Connell 3rd, J., Remis, J., Robles-Colmenares, Y., Miercke, L.J., and Stroud, R.M. (2004) Mechanism of ammonia transport by Amt/MEP/Rh: structure of AmtB at 1.35 A. *Science.* **305**: 1587–1594.

Larimer, F.W., Chain, P., Hauser, L., Lamerdin, J., Malfatti, S., Do, L., et al. (2004) Complete genome sequence of the metabolically versatile photosynthetic bacterium *Rhodopseudomonas palustris*. *Nat. Biotechnol.* **22**: 55–61.

LaSarre, B., McCully, A.L., Lennon, J.T., and McKinlay, J.B. (2017) Microbial mutualism dynamics governed by dose-dependent toxicity of cross-fed nutrients. *ISME J* **11**: 337–348.

McKinlay, J.B., Oda, Y., Ruhl, M., Posto, A.L., Sauer, U., and Harwood, C.S. (2014) Non-growing *Rhodopseudomonas palustris* increases the hydrogen gas yield from acetate by shifting from the glyoxylate shunt to the tricarboxylic acid cycle. *J. Biol. Chem.* **4**: 1960–1970.